

PathletRL++: Optimizing Trajectory Pathlet Extraction and Dictionary Formation via Reinforcement Learning

GIAN ALIX*, York University, Canada
 ARIAN HAGHPARAST*, York University, Canada
 MANOS PAPAGELIS, York University, Canada

Advances in tracking technologies have spurred the rapid growth of large-scale trajectory data. Building a compact collection of pathlets, referred to as a *trajectory pathlet dictionary*, is essential for supporting mobility-related applications. Existing methods typically adopt a top-down approach, generating numerous candidate pathlets and selecting a subset, leading to high memory usage and redundant storage from overlapping pathlets. To overcome these limitations, we propose a bottom-up strategy that incrementally merges basic pathlets to build the dictionary, reducing memory requirements by up to 24,000 times compared to baseline methods. The approach begins with unit-length pathlets and iteratively merges them while optimizing utility, which is defined using newly introduced metrics of *trajectory loss* and *representability*. We develop a deep reinforcement learning framework, PATHLET_{RL}, which utilizes Deep Q-Networks (DQN) to approximate the utility function, resulting in a compact and efficient pathlet dictionary. Experiments on both synthetic and real-world datasets demonstrate that our method outperforms state-of-the-art techniques, reducing the size of the constructed dictionary by up to 65.8%. Additionally, our results show that only half of the dictionary pathlets are needed to reconstruct 85% of the original trajectory data. Building on PATHLET_{RL}, we introduce PATHLET_{RL}++, which extends the original model by incorporating a richer state representation and an improved reward function to optimize decision-making during pathlet merging. These enhancements enable the agent to gain a more nuanced understanding of the environment, leading to higher-quality pathlet dictionaries. PATHLET_{RL}++ achieves even greater dictionary size reduction, surpassing the performance of PATHLET_{RL}, while maintaining high trajectory representability.

CCS Concepts: • **Information systems** → **Spatial-temporal systems**; • **Human-centered computing** → **Ubiquitous and mobile computing**; • **Computing methodologies** → **Machine learning**.

Additional Key Words and Phrases: mobility data analytics, mobile computing, spatial data mining, pathlets

ACM Reference Format:

Gian Alix, Arian Haghparsat, and Manos Papagelis. 2024. PathletRL++: Optimizing Trajectory Pathlet Extraction and Dictionary Formation via Reinforcement Learning. 1, 1 (December 2024), 37 pages. <https://doi.org/XXXXXXXX.XXXXXXX>

1 INTRODUCTION

Motivation & Problem of Interest. The development of technology for gathering and tracking location data has led to the accumulation of vast amounts of trajectory data, consisting of spatial and temporal information of moving objects, such as persons or vehicles. Mining trajectory data to

*Both authors contributed equally to this research.

Authors' addresses: Gian Alix, York University, Toronto, Canada, gcalix@eecs.yorku.ca; Arian Haghparsat, York University, Toronto, Canada, arianhgh@my.yorku.ca; Manos Papagelis, York University, Toronto, Canada, papaggel@eecs.yorku.ca.

Permission to make digital or hard copies of all or part of this work for personal or classroom use is granted without fee provided that copies are not made or distributed for profit or commercial advantage and that copies bear this notice and the full citation on the first page. Copyrights for components of this work owned by others than the author(s) must be honored. Abstracting with credit is permitted. To copy otherwise, or republish, to post on servers or to redistribute to lists, requires prior specific permission and/or a fee. Request permissions from permissions@acm.org.

© 2024 Copyright held by the owner/author(s). Publication rights licensed to ACM.

XXXX-XXXX/2024/12-ART \$15.00

<https://doi.org/XXXXXXXX.XXXXXXX>

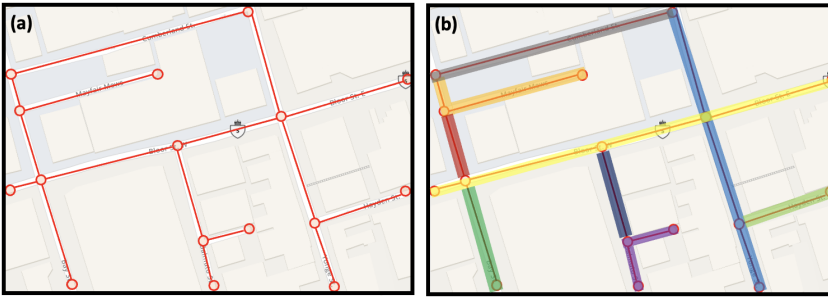


Fig. 1. (a) Graph representation of a small area in Toronto¹; (b) Example of various-length edge-disjoint pathlets in (a).

find interesting patterns is of increased research interest due to a broad range of useful applications, including analysis of transportation systems [31], human mobility [43], location-based services [57], spatiotemporal epidemics [3, 38, 39] and more. There are several technical problems in trajectory data mining that researchers and practitioners have focused on in recent years, including trajectory similarity [12], clustering [17], classification [4], prediction [55] and simplification [52].

A few comprehensive surveys on the topic can be found in Zheng [62], Alturi et al. [6], and Hamdi et al. [16]. In this research, we focus on the problem of constructing a small set of basic building blocks that can represent a wide range of trajectories, known as a (*trajectory*) *pathlet dictionary* (PD). The term *pathlet* appears in the literature by many names, such as *subtrajectories*, *trajectory segments*, or *fragments* [1, 8, 26, 36, 41, 59]. For consistency, we will use the term *pathlets* to denote these building blocks.

The Broader Impact. Effectively constructing pathlet dictionaries is of increased research and practical interest due to a broad range of tasks and applications that can use it, such as route planning [56], travel time prediction [18], personalized destination prediction [54], trajectory prediction [55], and trajectory compression [60] (see Appendix A for a supplementary discussion of these applications).

The State of the Art & Limitations. Many existing works frame the problem of analyzing and deriving pathlets as a (sub)trajectory clustering problem, where (sub)trajectory clusters represent popular paths (the pathlets) [1, 22, 46]. A few works considered an integer programming formulation with constraints to solve the problem [8, 26]. Some works designed their pathlets based on a route “representativeness” criterion [36, 51]. Unfortunately, these existing works suffer some limitations. For example, Chen et al. [8] assumes that the datasets used are noise-free. Zhou et al.’s [63] bag-of-segments method requires that trajectory segments are of fixed length. Van Krevald et al. [46] demands input trajectories to have the same start/endpoints. The cluster centroids in (sub)trajectory clustering methods [1, 22, 46, 49] do not necessarily reflect real roads in the road network. In addition, Wang et al. [51] demonstrated empirically that these clustering methods are computationally slow. In spite of runtime improvements, [51] also requires the user to provide some budget constraint B in the route representative discovery task, a domain-specific parameter that requires domain expert knowledge. Another related method is TRACULUS [22] that requires pathlets to be straight line segments, which is not always the case in real road maps. In addition, all these works do not constraint pathlets to be *edge-disjoint*; two pathlets are said to be edge-disjoint if they don’t share any edge. Therefore, existing works allow pathlets in the dictionary to (partially) overlap. These methods, by design, follow a top-down approach in constructing a dictionary. This involves forming all possible pathlet candidates first, by considering pathlets of various configurations and

¹Downtown Toronto maps taken from <https://www.mapquest.com/>

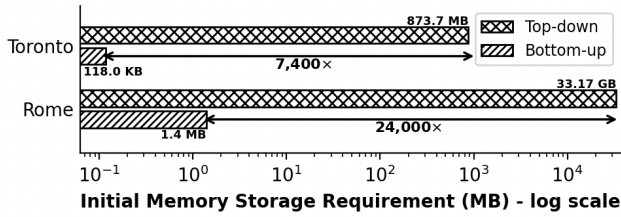


Fig. 2. The memory required by top-down (existing) methods that use overlapping pathlets can be reduced by our proposed bottom-up solution that use edge-disjoint pathlets.

sizes, and then eliminating candidates to form a smaller sized dictionary that consists of only the most important ones (e.g., the most popular). While simple and intuitive, its main limitation is the need for a large memory to initially store the large number of pathlets, most of which are redundant. This also limits its applicability in real-world settings, particularly when dealing with large road networks and trajectory data, as the number of initial candidates can quickly become overwhelming.

Our Approach & Contributions. To address these limitations, we propose a bottom-up approach for constructing a pathlet dictionary that complies with edge-disjoint pathlets (see Fig. 1) and reduces memory storage requirement. In Fig. 2 for instance, we illustrate how our proposed approach saves up to $\sim 24K\times$ less memory space than existing methods for storing the initial pathlets (see Experiment (Q2) for full details, with Appendix C presenting a more theoretical proof). The key idea of our approach is to initialize unit-length pathlets & iteratively merge them to form longer, higher-order ones, while maximizing utility [2, 28]. Longer pathlets are preferred (over shorter ones) as they hold more spatiotemporal information, such as mobility patterns in trajectories [8]. A deep reinforcement learning method is proposed to approximate the utility function.

A summary of our contributions is provided below:

- We introduce a more strict definition of a pathlet than in previous works to comply with edge-disjoint pathlets. This enables a bottom-up approach for constructing pathlet dictionaries that reduces memory storage needs.
- We introduce two novel metrics, namely *trajectory loss* and *trajectory representability*, which allow us to more comprehensively evaluate the utility of a pathlet and the overall quality of a constructed pathlet dictionary.
- We formulate the problem of *pathlet dictionary construction* as a utility maximization problem, where shorter pathlets are merged to form a set of longer ones with higher utility.
- We propose PATHLET_{RL}, a deep reinforcement learning method that utilizes a Deep Q Network (DQN) policy to approximate the utility function of constructing a pathlet dictionary. To the best of our knowledge, this is the first attempt to employ a deep learning method for the problem.
- We address the limitations of the original PATHLET_{RL} model by introducing optimization techniques to improve the quality and stability of the constructed pathlet dictionaries, ensuring better trade-offs between key objectives in trajectory modeling.
- We introduce PATHLET_{RL++}, which extends PATHLET_{RL} by incorporating a richer state representation and a more robust reward function to optimize decision-making during pathlet merging. This extension significantly improves the stability and quality of the constructed pathlet dictionary.
- We demonstrate empirically that the dictionary constructed by our PATHLET_{RL} and its extensions is of superior quality compared to those constructed by traditional non-learning-based methods. Our method reduces the size of the dictionary by up to 65.8% compared to other methods.

Symbol	Definition
τ and \mathcal{T}	A trajectory τ and a set of trajectories \mathcal{T}
$\mathcal{G}\langle\mathcal{V}, \mathcal{E}\rangle$	Road network with intersections \mathcal{V} and segments \mathcal{E}
ρ and \mathcal{P}	A pathlet ρ and a pathlet set \mathcal{P}
$\mathcal{G}_\rho\langle\mathcal{V}_\rho, \mathcal{E}_\rho\rangle$	The pathlet graph representation of road network \mathcal{G}
$\Psi(\rho)$	The neighbors of pathlet ρ
$\Phi(\tau)$	The pathlet-based representation of a trajectory τ
$\Lambda(\rho)$	The trajectory traversal set of a pathlet ρ
$\mu(\tau)$	The trajectory representability of trajectory τ
L_{traj}	The trajectory loss
\mathbb{S}	The pathlet dictionary
ϕ	The avg # of pathlets representing each τ in \mathcal{T}

Table 1. Summary of notation used in this work

Moreover, using only half of the pathlets in the dictionary suffices to reconstruct 85% of the original trajectory data.

- We open-source our code to encourage reproducibility².

Paper Organization. The remainder of the paper is organized as follows. Section 2 presents preliminaries and a formal definition of the problem. Section 3 outlines our methodology and the details of the proposed approach. Section 4 describes the experimental setup, presents the results, and provides insightful discussions. Section 5 introduces optimizations and extensions to the original PATHLETRL framework. We review related work in Section 6 and conclude in Section 7.

2 PRELIMINARIES & PROBLEM DEFINITION

In this section, we briefly introduce some definitions and notations (see Table 1). Then we formally define the problem of interest.

2.1 Primary Definitions and Notations

Definition 2.1 (Trajectory). Let $\mathbf{O} = \{o_1, o_2, \dots, o_{|\mathbf{O}|}\}$ be a set of moving objects in a certain geographic map $\mathcal{M} \subset \mathbb{R}^2$. A *trajectory* τ of a single object $o \in \mathbf{O}$ can be represented as a sequence of time-enabled geo-coordinate points: $\tau = \langle (x_1, y_1, t_1), \dots, (x_{|\tau|}, y_{|\tau|}, t_{|\tau|}) \rangle$, where each x_i and y_i represents o 's longitudinal and latitudinal coordinates at a specific time instance $t_i \in [0, T]$. We let $|\tau|$ be its length, or the # of time-enabled points for the trajectory of o . Moreover, we let *trajectory (data) set* \mathcal{T} consist of all trajectories of all $o \in \mathbf{O}$: $\mathcal{T} = \bigcup_{o \in \mathbf{O}} \mathcal{T}_o$, with \mathcal{T}_o as the set of all o 's trajectories.

Definition 2.2 (Road Network). We denote by $\mathcal{G}\langle\mathcal{V}, \mathcal{E}\rangle$ the *road network* within map \mathcal{M} , where \mathcal{V} and $\mathcal{E} \subseteq \mathcal{V} \times \mathcal{V}$ represents \mathcal{G} 's set of road intersections (nodes) and segments (edges) respectively.

Trajectory points (GPS traces) outside \mathcal{M} are filtered out as a preprocessing step. The remaining trajectories also require to be map-matched (see Appendix D for details). With map-matched data, we can now formalize the fundamental building block in this work.

Definition 2.3 (Pathlet). A *pathlet* ρ is defined as any sub-path in the road network \mathcal{G} , with \mathcal{P} being the set of all such pathlets.

In our work, we consider *edge-disjoint* pathlets, s.t. no two $\rho_1, \rho_2 \in \mathcal{P}$ share any edge. For simplicity, we assume *discrete* pathlets – meaning they begin and end at an intersection (a node in

²<https://github.com/Arianhgh/PathletRL>

the graph, with either start/endpoints at $\rho.s/\rho.e$, but the work can easily be generalized to include *continuous* pathlets that drop this restriction.

Definition 2.4 (Pathlet Length³). Denoted by ℓ , this represents pathlet ρ 's path length in the road network.

The smallest unit of the pathlet has length $\ell = 1$. Moreover, we restrict all pathlets $\rho \in \mathcal{P}$ to be of length $\ell \leq k$, for some user-defined k . In this case, we say that \mathcal{P} is a **k -order pathlet set**.

Definition 2.5 (Pathlet Graph). The *pathlet graph* $\mathcal{G}_p(\mathcal{V}_p, \mathcal{E}_p)$ of a road network $\mathcal{G}(\mathcal{V}, \mathcal{E})$ depicts the road network's pathlets, where the road intersections represent the nodes $\mathcal{V}_p \subseteq \mathcal{V}$ and the road segments connecting road intersections as the edges $\mathcal{E}_p \subseteq \mathcal{E}$.

Fig. 1(a), for example, represents the pathlet graph representation of a small area in Toronto. In our work, we consider an initial pathlet graph where each pathlet has length $\ell = 1$.

Definition 2.6 (Pathlet Neighbors). Given a pathlet $\rho \in \mathcal{P}$, its neighbor pathlets, denoted by $\Psi(\rho)$, are all other pathlets $\rho' \in \mathcal{P} \setminus \{\rho\}$ who share the same start/endpoints with that of ρ :

$$\Psi(\rho) = \bigcup_{\rho' \in \mathcal{P} \setminus \{\rho\}, (\rho.s \in \{\rho'.s, \rho'.e\}) \vee (\rho.e \in \{\rho'.s, \rho'.e\})} \rho'$$

For example, the grey pathlet in Fig. 1(b) has two neighbors: the orange & blue pathlets.

Definition 2.7 (Pathlet-based Representation of a Trajectory). A trajectory $\tau \in \mathcal{T}$ can be represented based on some subset of pathlets $\mathcal{P}_{sub} \subseteq \mathcal{P}$. Moreover, the pathlets in \mathcal{P}_{sub} can be concatenated in some sequence resulting into the path traced by τ on the road network \mathcal{G} . We denote this by $\Phi(\tau) = \{\rho^{(1)}, \rho^{(2)}, \dots, \rho^{(|\mathcal{P}_{sub}|)}\}$, where $\rho^{(i)} \in \mathcal{P}_{sub}$ denotes the i th pathlet in the sequence that represents the pathlet-based representation for τ .

Based on this, it is also possible to define a trajectory's pathlet length, which we initially set before constructing the pathlet graph. Each trajectory $\tau \in \mathcal{T}$ has pathlet length equal to $\sum_{\rho \in \Phi(\tau)} \ell(\rho)$, whose value remains static for the rest of our algorithm.

Definition 2.8 (Trajectory Traversal Set of a Pathlet). Let $\Lambda(\rho)$ be the set of all trajectories $\tau \in \mathcal{T}$ that *pass* or *traverse* pathlet $\rho \in \mathcal{P}$. This can also be written as $\Lambda(\rho) = \{\tau \mid \forall \tau \in \mathcal{T}, \rho \in \Phi(\tau)\}$.

We can also assign weights ω to pathlets. In the unweighted case, all pathlets are weighed equally; while in the weighted version, pathlets are weighed equal to the # of trajectories traversing a pathlet, i.e., $\omega(\rho) = |\Lambda(\rho)|$, or $\frac{|\Lambda(\rho)|}{|\mathcal{T}|}$ when normalized. These weights indicate each pathlet's importance in the road network/pathlet graph.

2.2 Novel Trajectory Metrics

We can now introduce some novel metrics to allow us to more comprehensively evaluate our pathlets and pathlet dictionaries.

Definition 2.9 (Trajectory Representability⁴). The (trajectory) representability $\mu \in [0\%, 100\%]$ of a trajectory τ denotes the % of τ that can be represented using pathlets in pathlet set \mathcal{P} .

Clearly, the pathlet-based representation of τ is directly related to its representability, i.e., $\mu(\tau) = \sum_{\rho \in \Phi(\tau)} \frac{\ell(\rho)}{|\tau|}$, for the unweighted case and $\mu(\tau) = \sum_{\rho \in \Phi(\tau)} \omega(\rho)$, for the weighted version.

Definition 2.10 (Trajectory Loss). We define the *trajectory loss* L_{traj} to be the # of trajectories $\forall \tau \in \mathcal{T}$ that have representability value $\mu = 0\%$, i.e., $L_{traj} = |\{\tau \mid \tau \in \mathcal{T}, \mu(\tau) = 0\}|$. We can also

³Not to confuse with a road segment's length that represents the measure depicting its actual physical distance, the pathlet length can be derived based on graph context.

⁴Not to be confused with *representativeness* that describes the capability of a trajectory to represent other similar nearby trajectories, *representability* depicts how much a trajectory can be reconstructed given our pathlets.

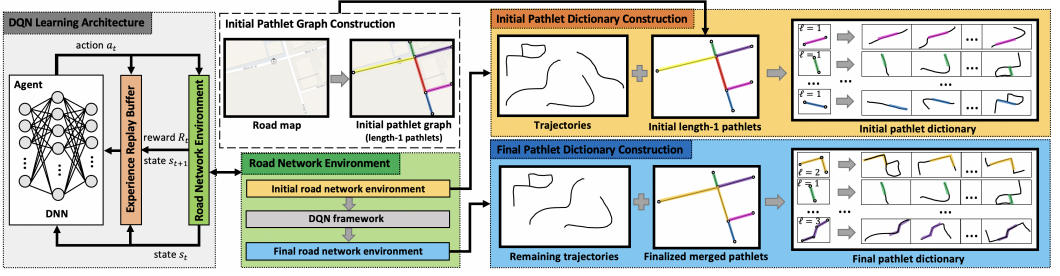


Fig. 3. The overall architecture (including the constructed PDs) of our proposed PATHLETRL model

describe these trajectories as "lost" or "discarded" from the given trajectory set \mathcal{T} , and we may also depict this number as a %.

The relevance and impact of these two metrics will become clear as we go over the methodology in finer details.

2.3 Problem Definition

Before formalizing the problem, we first introduce the *pathlet dictionary* and some optimization definitions.

Definition 2.11 (Pathlet Dictionary). A (trajectory) pathlet dictionary (PD) is a data structure that stores pathlets $\rho \in \mathcal{P}$ (keys), and their associated trajectory traversal set $\Lambda(\rho)$ (values).

See Fig. 3 (the righthand boxes inside the orange & blue panels) for an illustrative example of a PD. We are interested in constructing a PD that aims to achieve one or a combination of the following:

- (O1) Minimal size of candidate pathlet set \mathbb{S} , or the candidate set with the least possible number of pathlets (i.e., $\min |\mathbb{S}|$)
- (O2) Minimal ϕ , or the avg # of pathlets representing each trajectory $\tau \in \mathcal{T}$ (i.e., $\min \phi = \min \frac{1}{|\mathcal{T}|} \sum_{\tau \in \mathcal{T}} |\Phi(\tau)|$)
- (O3) Minimal trajectory loss L_{traj} (i.e., $\min L_{traj}$)
- (O4) Maximal $\bar{\mu}$, or the average representability values of the remaining trajectories in \mathcal{T} (i.e., $\max \bar{\mu} = \max \frac{1}{|\mathcal{T}|} \sum_{\tau \in \mathcal{T}} \mu(\tau)$)

In other words, the objective function that we wish to optimize is based on the four objectives above – which can be modelled by:

$$\min_{\sum_i \alpha_i = 1} \left(\alpha_1 |\mathbb{S}| + \alpha_2 \frac{1}{|\mathcal{T}|} \sum_{\tau \in \mathcal{T}} |\Phi(\tau)| + \alpha_3 L_{traj} - \alpha_4 \frac{1}{|\mathcal{T}|} \sum_{\tau \in \mathcal{T}} \mu(\tau) \right) \quad (1)$$

where the α_i 's are user-defined objective weights.

Problem 1 (Pathlet Dictionary Construction). Given a road network $\mathcal{G}(\mathcal{V}, \mathcal{E})$ of a specific map \mathcal{M} , a trajectory set \mathcal{T} , max pathlet length k , max trajectory loss M , and avg trajectory representability threshold $\hat{\mu}$, construct a k -order pathlet dictionary \mathbb{S} . The dictionary \mathbb{S} consists of edge-disjoint pathlets with lengths of at most k , and achieves the max possible utility according to some utility function as depicted in Equation (1), such that $L_{traj} < M$ and $\bar{\mu} \geq \hat{\mu}$.

Algorithm 1: PathletRL: Trajectory Pathlet Dictionary Construction

Input: Road Network $\mathcal{G}(V, E)$, Trajectory Set \mathcal{T} , Maximum Pathlet Length k , Trajectory Loss Threshold M , Average Representability Threshold $\mu_{\text{threshold}}$.

Output: Pathlet Dictionary \mathcal{S} for Representing \mathcal{T} .

```

1 Initialization:
2 Set the candidate set  $C = \emptyset$  for storing processed pathlets
3 Construct the pathlet graph  $\mathcal{G}_p$  from the input road network  $\mathcal{G}$ 
4 Identify neighbors for each pathlet and compute initial pathlet weights  $\omega_p$ 
5 For each trajectory  $t_i \in \mathcal{T}$ , compute initial trajectory coverage  $\phi$ , representability  $\mu$ 
6 Randomly select an initial pathlet  $p_{\text{current}} \in \mathcal{G}_p \setminus C$ 
7 while termination conditions not met do
8   if Trajectory loss  $L_{\text{traj}}$  exceeds  $M$  or  $\mu < \mu_{\text{threshold}}$  or  $\mathcal{G}_p \setminus C = \emptyset$  then
9     Terminate the episode and store the final pathlet dictionary  $\mathcal{S}$ ;
10  Observe current state  $s_t$  of  $\mathcal{G}_p$ ;
11  Select action  $a_t$  using the  $\epsilon$ -greedy policy from DQN;
12  if  $a_t = 0$  (Skip action) then
13    Mark current pathlet  $p_{\text{current}}$  as processed by adding it to  $C$ ;
14    if  $\mathcal{G}_p \setminus C \neq \emptyset$  then
15      Randomly select a new pathlet  $p_{\text{current}} \in \mathcal{G}_p \setminus C$ ;
16    else
17      Terminate the episode and store the final pathlet dictionary  $\mathcal{S}$ ;
18  else
19    Select neighboring pathlet  $p_{\text{neighbor}}$  based on action  $a_t$ ;
20    if Merging  $p_{\text{current}}$  and  $p_{\text{neighbor}}$  results in path length  $\leq k$  then
21      Merge pathlets to form a new pathlet  $p_{\text{merged}}$ ;
22      Update traversal set  $\Lambda(p_{\text{merged}})$  and pathlet graph  $\mathcal{G}_p$ ;
23      Recompute trajectory coverage  $\phi$ , representability  $\mu$ , and trajectory loss  $L_{\text{traj}}$ ;
24      Remove trajectories with zero coverage from  $\mathcal{T}$ ;
25      Update the set of unprocessed pathlets  $\mathcal{G}_p \setminus C$ ;
26      Set  $p_{\text{current}} = p_{\text{merged}}$ ;
27    else
28      Mark  $p_{\text{current}}$  as processed by adding it to  $C$ ;
29      if  $\mathcal{G}_p \setminus C \neq \emptyset$  then
30        Randomly select a new pathlet  $p_{\text{current}} \in \mathcal{G}_p \setminus C$ ;
31      else
32        Terminate the episode and store the final pathlet dictionary  $\mathcal{S}$ ;
33  Compute reward  $R_t$  based on changes in size  $|\mathcal{S}|$ , representability  $\mu$ , trajectory loss  $L_{\text{traj}}$ ,
    and average number of pathlets per trajectory  $\phi$ ;
34  Store transition  $(s_t, a_t, R_t, s_{t+1})$  in experience replay buffer;
35  Perform DQN update on the Q-network using sampled experiences;
36  Set next state  $s_{t+1}$ ;
37 Output: Pathlet dictionary  $\mathcal{S}$ 

```

3 METHODOLOGY

We now describe our methods to address the problem of interest (see Fig. 3 for its architecture). In particular, we describe the components of the proposed PATHLETRL model (**Pathlet** dictionary construction using trajectories with **Reinforcement Learning**). There are two main components: (1) the method responsible for extracting the candidate pathlet sets through a merging-based process, and (2) a deep reinforcement learning-based architecture for approximating the utility function of the merging process of (1).

3.1 Extracting Candidate Pathlets

In this section, we describe the algorithmic details for merging our edge-disjoint pathlets. The high-level idea of the algorithm is based on the theory of maximal utility [2, 28], i.e., iteratively merging (neighboring) pathlets until this brings forth little to no improvement on the *utility* (details of the utility are given later). The algorithm takes in as input a road network \mathcal{G} , a trajectory set \mathcal{T} operating within \mathcal{G} , the max threshold for the trajectory loss M , the trajectory representability threshold $\hat{\mu}$, and a positive integer k denoting the desired k -order pathlet graph. As output, it returns a pathlet dictionary (PD) that holds pathlet information as described in Definition 2.11. The extracted PD aims to satisfy the four objectives **(O1)**-**(O4)**. See Algorithm 1 for the pseudocode.

Initialization. The algorithm begins by setting up an empty candidate set $C = \emptyset$ to keep track of processed pathlets. It constructs the initial pathlet graph \mathcal{G}_p from the input road network \mathcal{G} , which consists of initial pathlets of length 1. For each trajectory $t_i \in \mathcal{T}$, it calculates the initial trajectory coverage ϕ and representability μ . An initial pathlet p_{current} is randomly chosen from the set of unprocessed pathlets $\mathcal{G}_p \setminus C$.

An Iterative Algorithm. The algorithm operates in a loop where, at each iteration, the agent observes the current state s_t of the environment and selects an action a_t using an ϵ -greedy policy from the Deep Q-Network (DQN). The actions are defined as follows:

- **Skip Action** ($a_t = 0$): The agent chooses to skip the current pathlet p_{current} , marking it as processed by adding it to C . If there are still unprocessed pathlets remaining (i.e., $\mathcal{G}_p \setminus C \neq \emptyset$), the agent randomly selects a new pathlet from this set to be the next p_{current} . Otherwise, the episode terminates, and the final pathlet dictionary \mathcal{S} is produced.
- **Merge Action** ($a_t > 0$): The agent selects a neighboring pathlet p_{neighbor} based on the action a_t to merge with the current pathlet p_{current} . If merging these two pathlets results in a new pathlet whose length does not exceed the maximum allowed length k , they are merged to form a new pathlet p_{merged} . The traversal set $\Lambda(p_{\text{merged}})$ and the pathlet graph \mathcal{G}_p are updated accordingly. Trajectories that now have zero coverage are removed from the trajectory set \mathcal{T} . The metrics ϕ , μ , and trajectory loss L_{traj} are recalculated. The agent then updates p_{current} to be the newly formed p_{merged} . If merging is not possible due to length constraints, the agent treats this as a skip action. At each iteration, the agent computes a reward R_t based on changes in the size of the pathlet dictionary $|\mathcal{S}|$, representability μ , trajectory loss L_{traj} , and the average number of pathlets per trajectory ϕ . The transition (s_t, a_t, R_t, s_{t+1}) is stored in the experience replay buffer, and the DQN updates its Q-network using sampled experiences. The loop continues until one of the termination conditions is met: the trajectory loss exceeds the threshold M , the average representability μ falls below the threshold $\mu_{\text{threshold}}$, or there are no unprocessed pathlets left. The final pathlet dictionary \mathcal{S} .

The Utility Function. To complete the description of the algorithm, we discuss the formulation of the utility function that we approximated using a learning-based method.

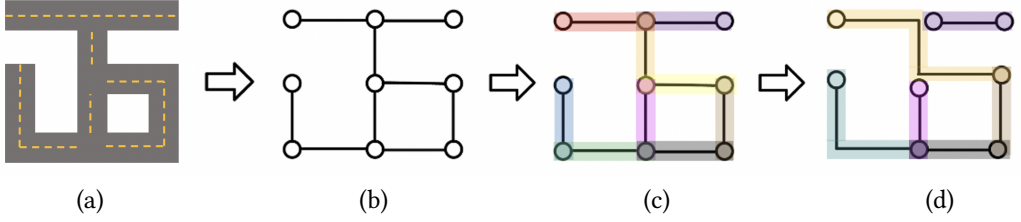


Fig. 4. An illustrative example of Example 3.1: (a) A toy example of a simple road network; (b) A grid representation of (a); (c) The initial pathlet graph representation (of length-1 pathlets) for the road network in (a); (d) The final (merged) pathlet graph representation after the completion of the pathlet-merging algorithm in Algorithm 1.

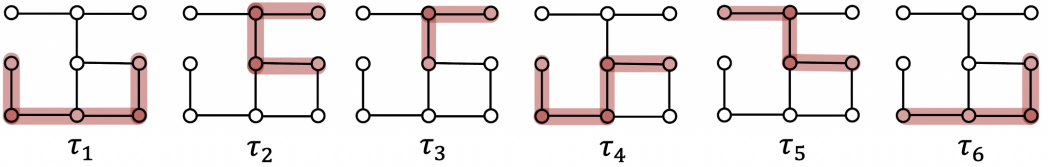


Fig. 5. An illustrative example of the paths (road segments) traversed by six trajectories $\{\tau_1, \tau_2, \tau_3, \tau_4, \tau_5, \tau_6\}$ (highlighted by maroon) from the road network of Example 3.1 as seen in Figure 4; see Table 3 that lists the sequential pathlet-based representations of each trajectory.

In particular, a reinforcement learning method is utilized to learn the (sequence of) actions (i.e., merge or don't merge pathlets) that would yield the highest possible utility. Specifically, we frame the utility function as a *reward function* that we aim to optimize (i.e., maximize). We discuss the details of this design in the next section.

With the pathlet dictionary constructed following this process of pathlet merging based on the utility theory, we can attain something like the one depicted in Figure 3 (bottom right figure). Now we provide a simple toy example of the algorithm.

EXAMPLE 3.1. *As edge-disjoint pathlets are non-overlapping, then a decision would have to be made when a pathlet is about to merge with one of its neighbor pathlets. As such, there is some advantages or gains by merging with a certain pathlet, but such action also comes with some cost. This is where trajectory representabilities and losses come in. More specifically, a trajectory's representability will drop when a portion of its trajectory cannot be represented due to a pathlet merging with one of its neighbors. To give a more concrete example, consider the snippet of a road network in Figure 4(a). Figure 4(b) illustrates its grid representation, and Figure 4(c) the (initial) pathlet graph representation, where we highlighted using various colors the nine pathlets in question. See the left image of Figure 6 for the labels of these pathlets and their color code in Table 2. Initially, our pathlet dictionary is composed of the following based on the six trajectories as highlighted by the maroon color on the grid graph in Figure 5 (their pathlet-based representations in Table 3):*

$$\begin{aligned} \rho_1 : \{\tau_5\} & \quad \rho_2 : \{\tau_2, \tau_3\} & \quad \rho_3 : \{\tau_2, \tau_3, \tau_5\} & \quad \rho_4 : \{\tau_2, \tau_4, \tau_5\} & \quad \rho_5 : \{\tau_1, \tau_4\} \\ \rho_6 : \{\tau_4\} & \quad \rho_7 : \{\tau_1, \tau_6\} & \quad \rho_8 : \{\tau_1, \tau_4, \tau_6\} & \quad \rho_9 : \{\tau_1, \tau_6\} \end{aligned}$$

After the entire merging process, the algorithm returns the following final dictionary – with its illustration in Figure 4(d), with their labels in Figure 6, their color codes in Table 2 and the trajectories' updated representabilities and pathlet-based representations in Table 3:

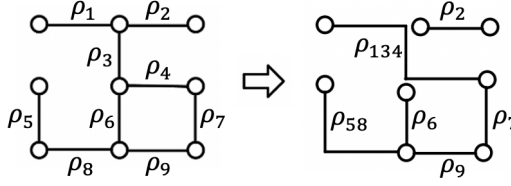


Fig. 6. Pathlet labels for the initial and final pathlet graph representations

Pathlet	Color
ρ_1	red
ρ_2	purple
ρ_3	orange
ρ_4	yellow
ρ_5	blue
ρ_6	pink
ρ_7	brown
ρ_8	green
ρ_9	grey
ρ_{134}	tangerine
ρ_{58}	aquamarine

Table 2. Color coding of the pathlets for the toy example in Example 3.1

Traj	Pathlet-based representation set Φ (Representability μ)	
	(Before merge)	(After merge)
τ_1	$\{\rho_5, \rho_8, \rho_9, \rho_7\}$ (100%)	$\{\rho_{58}, \rho_9, \rho_7\}$ (100%)
τ_2	$\{\rho_2, \rho_3, \rho_4\}$ (100%)	$\{\rho_2\}$ (33%)
τ_3	$\{\rho_3, \rho_2\}$ (100%)	$\{\rho_2\}$ (50%)
τ_4	$\{\rho_4, \rho_6, \rho_8, \rho_5\}$ (100%)	$\{\rho_6, \rho_{58}\}$ (75%)
τ_5	$\{\rho_4, \rho_3, \rho_1\}$ (100%)	$\{\rho_{134}\}$ (100%)
τ_6	$\{\rho_7, \rho_9, \rho_8\}$ (100%)	$\{\rho_7, \rho_9\}$ (67%)

Table 3. Pathlet-based representation set (and trajectory representabilities) of the provided toy example in Example 3.1

$$\rho_{134} : \{\tau_5\} \quad \rho_2 : \{\tau_2, \tau_3\} \quad \rho_{58} : \{\tau_1, \tau_4\} \quad \rho_6 : \{\tau_4\} \quad \rho_7 : \{\tau_1, \tau_6\} \quad \rho_9 : \{\tau_1, \tau_6\}$$

Note that pathlets ρ_1 , ρ_3 , and ρ_4 from initial pathlet graph merged to become pathlet ρ_{134} in the final pathlet graph (it is irrelevant in this example whether pathlet ρ_3 merged with ρ_1 or ρ_4 first). The same can be said for pathlets ρ_5 and ρ_8 to form pathlet ρ_{58} .

Initially, all trajectories have $\mu = 100\%$ representability values because all six trajectories can be represented by pathlets in the initial pathlet dictionary. However, after the entire merging process, we are left with some of the original six trajectories to have a lower μ value than the original representability value. Notice for example trajectory τ_1 ; its μ value did not drop because all the pathlets in its original pathlet-based representation Φ either have never merged, or have merged with a neighboring pathlet that also belongs to $\Phi(\tau_1)$. In other words, the entirety of trajectory τ_1 can still be represented by the pathlets in the final pathlet dictionary; this results into its representability being maintained at 100%. A similar story can be told for trajectory τ_5 . For the rest of the trajectories, the representabilities are lower. Looking at trajectory τ_2 for example whose $\Phi(\tau_2) = \{\rho_2, \rho_3, \rho_4\}$. However, after the algorithm, we only have $\Phi(\tau_2) = \{\rho_2\}$ left; the reason being is that pathlets ρ_1 , ρ_3 , and ρ_4 have all merged together to form ρ_{134} . But note that since ρ_1 does not represent τ_2 , then the merged ρ_{134} is not part of the $\Phi(\tau_2)$ after completing the iterative algorithm. As a result, it is expected for its trajectory representability to drop. The same story can be said for trajectories τ_3 , τ_4 and τ_6 .

Remark. One can imagine that the representabilities of the trajectories can potentially drop at each step of the iterative algorithm, until it drops to zero. In the event that a trajectory's representability reaches zero, it is removed from the trajectory set and counted as a *trajectory loss*. Now this is a soft version of what is considered to be a trajectory loss. There is a harder, stricter variation, where the notion of trajectory representability is eliminated from the picture, (i.e., a trajectory

losing only a small portion of its representability due to a pathlet merge action meant that the entire trajectory is considered lost), entails throwing excessive trajectories and can be fatal to the performance of the model and the algorithm. Intuitively, one might not desire discarding an entire trajectory when (say only 1% of the trajectory) cannot be represented due to the pathlet merge. The experimental evaluations later will demonstrate the essence of this soft version that takes trajectory representability into account.

THEOREM 3.1 (TRAJECTORY REPRESENTABILITY THEOREM). *At any step i of the iterative Algorithm 1, then the trajectory representability μ of some trajectory $\tau \in \mathcal{T}$ by the end of that iteration i is equal to:*

$$\mu_i(\tau) = \frac{\sum_{\rho' \in \Phi_i(\tau)} \ell(\rho')}{\sum_{\rho \in \Phi_0(\tau)} \ell(\rho)} \quad (2)$$

where Φ_0 and Φ_i are the pathlet-based representation of trajectory τ in the initial (iteration 0) and iteration i of the iterative algorithm respectively.

The above theorem provides a formula for how to compute a trajectory's representability value μ at some iteration i of the algorithm. We refer the reader to Appendix B where we provide a complete proof for this theorem.

3.2 Background on Reinforcement Learning

For readers already familiar with reinforcement learning and Deep Q-Networks (DQN), you may proceed directly to Section 3.3. For those new to the topic, we provide a brief overview of essential concepts to facilitate understanding of our framework.

Markov Decision Process (MDP). An MDP models decision-making where outcomes are partly random and partly under the control of an agent. It consists of:

- \mathcal{S} : Set of possible states.
- \mathcal{A} : Set of actions available to the agent.
- $\mathcal{P}(s' | s, a)$: Transition probability from state s to s' after action a .
- $\mathcal{R}(s, a, s')$: Immediate reward received after transitioning to state s' from s using action a .
- $\gamma \in [0, 1]$: Discount factor for future rewards.

The agent aims to learn a policy π that maximizes the expected cumulative reward.

Policy (π). A policy maps states to actions. It can be deterministic or stochastic, assigning probabilities to actions. The goal is to find a policy that maximizes the expected return.

Value Functions. The value function $V^\pi(s)$ estimates the expected return starting from state s under policy π :

$$V^\pi(s) = \mathbb{E}_\pi \left[\sum_{k=0}^{\infty} \gamma^k r_{t+k} \mid s_t = s \right]$$

Similarly, the action-value function $Q^\pi(s, a)$ estimates the expected return after taking action a in state s :

$$Q^\pi(s, a) = \mathbb{E}_\pi \left[\sum_{k=0}^{\infty} \gamma^k r_{t+k} \mid s_t = s, a_t = a \right]$$

Iterative Learning in Reinforcement Learning. Reinforcement learning is inherently iterative. The agent interacts with the environment in a sequence of time steps. At each time step t :

- (1) The agent observes the current state s_t .
- (2) Based on its policy π , the agent selects an action a_t .

- (3) The environment transitions to a new state s_{t+1} according to the transition probability $\mathcal{P}(s_{t+1} | s_t, a_t)$.
- (4) The agent receives a reward $r_t = \mathcal{R}(s_t, a_t, s_{t+1})$.
- (5) The agent updates its policy π to improve future actions, often using the observed reward and state transitions.

Through this iterative process, the agent learns from the consequences of its actions, adjusting its policy to maximize cumulative rewards over time. This learning continues until the agent's policy converges to an optimal or satisfactory level of performance.

Q-Learning and Deep Q-Networks (DQN). Q-learning is an algorithm where the agent learns the optimal action-value function $Q^*(s, a)$ by iteratively updating its estimates based on the Bellman equation:

$$Q(s_t, a_t) \leftarrow Q(s_t, a_t) + \alpha \left[r_t + \gamma \max_{a'} Q(s_{t+1}, a') - Q(s_t, a_t) \right]$$

where α is the learning rate.

Deep Q-Networks (DQN) extend Q-learning to handle large or continuous state spaces by using a neural network to approximate the Q -function. The iterative learning involves:

- Collecting experiences (s_t, a_t, r_t, s_{t+1}) by interacting with the environment.
- Storing experiences in a replay buffer.
- Sampling mini-batches from the replay buffer to train the neural network.
- Updating the network parameters to minimize the difference between predicted and target Q -values.

This process allows the agent to learn effective policies even in complex environments.

3.3 Reinforcement Learning Framework

Building upon the reinforcement learning concepts introduced earlier, we now detail how we apply RL to the pathlet merging problem. Our goal is to train an agent to decide whether to merge or keep specific pathlets in the graph, optimizing the trade-off between the objectives mentioned in section 2.3.

Agent. The agent interacts with the pathlet graph by selecting actions that alter its structure. It aims to learn a policy that maximizes cumulative rewards, effectively simplifying the graph while maintaining high trajectory representability.

States. Each state s_t captures the current configuration of the pathlet graph. We represent the state as a 4-tuple:

$$(S_1, S_2, S_3, S_4)$$

where:

- S_1 : Number of pathlets in the graph ($|\mathbb{S}|$).
- S_2 : Average number of pathlets needed to represent trajectories.
- S_3 : Trajectory loss metric L_{tra_j} , indicating the proportion of trajectories that cannot be accurately represented.
- S_4 : Average trajectory representability $\bar{\mu}$.

This state representation encapsulates key factors affecting our optimization objectives.

The Actions. At each time t , the agent has a choice of two discrete actions on the currently processed pathlet ρ , as expressed by the action space $\mathcal{A} = \{\text{KEEP}, \text{MERGE}\}$. In other words, KEEP action suggests that the current pathlet ρ should be kept and not be merged with any one of its neighbors. As a result, Algorithm 1 puts the current pathlet ρ in the processed set and then selects a new pathlet to process, performing one of the two actions in the action space on that new pathlet.

The MERGE action should however merge the current pathlet ρ with one of its $|\Psi(\rho)|$ neighbors. For that, the agent would need to decide on which neighbor in the set $\Psi(\rho)$ to merge with. Thus, the action space can succinctly be written as:

$$\mathcal{A} = \bigcup_{\forall \hat{\rho} \in \Psi(\rho)} \text{MERGE}(\rho, \hat{\rho}) \cup \{\text{KEEP}(\rho)\}$$

The Reward Function. We formulate our reward function R based on the optimization equation defined in Equation (1):

$$\max_{a_t} \mathbb{E} \left[\left(-\alpha_1 |\mathbb{S}| - \alpha_2 \frac{1}{|\mathcal{T}|} \sum_{\tau \in \mathcal{T}} |\Phi(\tau)| - \alpha_3 L_{\text{traj}} + \alpha_4 \frac{1}{|\mathcal{T}|} \sum_{\tau \in \mathcal{T}} \mu(\tau) \right) \right] \quad (3)$$

Whenever the RL agent performs an action a_t in the pathlet graph environment, the environment provides back feedback to it in the form of instantaneous rewards $\{r_t\}_{t=0}^T$:

$$r_t = -\alpha_1 \Delta |\mathbb{S}| - \alpha_2 \Delta \phi - \alpha_3 \Delta L_{\text{traj}} + \alpha_4 \Delta \bar{\mu}$$

where $\Delta \odot$ represents the change of \odot 's value in the previous and current timesteps. In the end, the agent receives the total sum of these instantaneous rewards, plus the final reward as depicted in Equation (3). Note that in order for the agent to realize the importance of both immediate and long-term future rewards, a user-defined *discounted rate factor* $\gamma \in [0, 1]$ was introduced.

The Policy and DQN Implementation. To handle the challenge of a continuous state space, we employ a Deep Q-Network (DQN) to approximate the optimal action-value function. The agent's policy π aims to select actions that maximize the expected cumulative reward:

$$Q^\pi(s_t, a_t) = \mathbb{E} [R_t | s_t, a_t]$$

Instead of maintaining a Q -table, which is impractical due to the size of our state and action spaces, the DQN uses a neural network to estimate Q -values. The network takes the state s_t as input and outputs estimated Q -values for possible actions a_t . By training this network, the agent learns an effective policy for deciding when to merge or keep pathlets, aiming to maximize the cumulative reward defined by our objectives.

Experience Replay and Training. During training, the agent interacts with the environment and collects experiences in the form of transitions (s_t, a_t, r_t, s_{t+1}) . To improve learning stability and efficiency, we utilize an experience replay buffer [14] where these transitions are stored. The agent samples mini-batches from this buffer to train the neural network, which helps break the temporal correlations between sequential data. An ϵ -greedy strategy is employed during data collection to balance exploration and exploitation: the agent selects a random action with probability ϵ , and the action with the highest estimated Q -value otherwise. The network is trained to minimize the Huber loss between the predicted Q -values and the target Q -values computed from the sampled experiences. This loss function is distinct from our trajectory loss metric, which assesses the number of trajectories that cannot be represented by the current set of pathlets.

3.4 Space Complexity Analysis

One of the main motivations for why edge-disjoint pathlets have been used together with bottom-up approaches is due to the reduced memory storage requirements that is necessary to initialize pathlets, in contrast with previous works that utilize top-down schemes with overlapping, redundant pathlets. In fact, we provide a space complexity analysis of top-down approaches and compare this with the proposed bottom-up methods through the following theorem (see Appendix C for the proof).

THEOREM 3.2 (INITIAL MEMORY STORAGE REQUIREMENT THEOREM). *The memory space that is required by top-down methods for initializing a pathlet dictionary has a quadratic $\Theta(n^2)$ bound, with n as the number of segments of the road network. Bottom-up schemes on the other hand, such as the proposed PATHLETRL, requires only an initial $\Theta(n)$ amount of memory space, with n as the number of initial length-1 pathlets.*

4 EVALUATION

In this section, we present the details of our experimental setup for evaluating our proposed method. We aim to analyze and evaluate our models based on the following research questions:

- (Q1) How does PATHLETRL compare with the SOTA methods, in terms of the quality of the extracted PDs?
- (Q2) How much memory does the bottom-up approach save compared to top-down methods?
- (Q3) How much improvement and how much more effective is our PATHLETRL model against its ablation variations?
- (Q4) What is the distribution of pathlet lengths in the obtained dictionary in our PATHLETRL model?
- (Q5) How effective is the constructed PD in reconstructing the original trajectories?
- (Q6) What is the sensitivity of the user-defined parameters $[\alpha_1, \alpha_2, \alpha_3, \alpha_4]$ in the performance of our PATHLETRL model?
- (Q7) How do the hyper-parameters such as the maximum length of pathlets and the average trajectory representability threshold impact the performance and efficiency of PATHLETRL?

4.1 Datasets

We utilize two datasets that each depict a different map scenario (see Appendix F for its complete statistics, and Appendix G for a brief discussion about the data's privacy concerns). We used real world maps of two metropolitan cities, Toronto⁵ and Rome through the OpenStreetMaps⁶. A realistic synthetic vehicular mobility datasets for the TORONTO map was generated using the SUMO mobility app simulator⁷ (3.7 hrs). Moreover, larger-scale, real-world taxi cab trajectories (first week of February 2014) were taken from CRAWDAD [7], an archive site for wireless network and mobile computing datasets, to form the ROME dataset. We split our trajectory sets into 70% training and 30% testing, where the training data was used to construct our pathlet dictionaries and the remainder for evaluation.

4.2 Experimental Parameters

Refer to Appendix H for full details of the implementation. To implement the RL architecture, we used a deep neural network that consists of the following parameters. It comprises of three hidden fully-connected layers of 128, 64 and 32 hidden neurons. The ReLU activation function has been employed, optimized by Adam with a learning rate of 0.001. We also use a 0.2 dropout in the network, together with the Huber loss function. More specific to the DQN's parameters, we have $m = 5$ episodes for each of the $n = 100$ iterations. The size of the experience replay buffer is 100,000 and the memory minibatch size is 64. Our agent also uses a discount factor $\gamma = 0.99$. Moreover, we use $k = 10$ for the k -order candidate set, $M = 25\%$ maximum trajectory loss and $\hat{\mu} = 80\%$ average representability threshold. We also set $\alpha_i = \frac{1}{4}, \forall i$, which denotes equal importance for each of the four objectives as depicted in Equation (3).

⁵<https://www.toronto.ca/city-government/data-research-maps/open-data/>

⁶<https://www.openstreetmap.org/>

⁷Simulation of Urban MObility: <https://www.eclipse.org/sumo/>

PATHLETRL ALGORITHM	Representability Measure	Weighted Networks	Deep Learning Policy
PATHLETRL-NR	✗	✓	✓
PATHLETRL-RND	✓	✓	✗
PATHLETRL-UNW	✓	✗	✓
PATHLETRL (OURS)	✓	✓	✓

Table 4. Features of the proposed PATHLETRL models, alongside its ablation baselines.

4.3 Baselines

We introduce the following baselines (see Appendix I for a discussion on baseline choice). The first two are SOTA (top-down-based) baselines, while the last three are ablation versions of our proposed model. Table 4 depicts the features withheld in each ablation variation to demonstrate the feature’s importance and effectiveness.

Chen et al. [8]. The very first paper that introduces the notion of pathlets. This method frames the problem as an integer programming formulation, that is solvable using dynamic programming.

Agarwal et al. [1]. Framing PD extraction as a subtrajectory clustering problem, where subtrajectory clusters are treated as pathlets, they use *pathlet-cover* inspired from the popular *set-cover* algorithm.

SGT. The *Singleton* baseline considers all initial length-1 pathlets (the original road map), without merging any pathlets.

PATHLETRL-RND. This version of PATHLETRL does not support Deep Q Networks and does not utilize a DQN agent. Actions at each episodic timestep are taken uniformly at random.

PATHLETRL-NR. Trajectory representability is absent under this ablation. If a pathlet traversed by some trajectory τ merges with another pathlet that is not traversed by this τ , then there no longer exists a subset of pathlets in the pathlet set that can represent τ ; as a result, we immediately discard trajectory τ .

PATHLETRL-UNW. This version of PATHLETRL is applied to a pathlet graph environment where all pathlets are equally weighted.

4.4 Evaluation Metrics

To evaluate model performance, we consider the following metrics that will measure the quality of the extracted pathlet dictionaries. Note that [↓] ([↑]) indicate that lower (higher) values are better.

- (1) $|\mathcal{S}|$, the size of the pathlet dictionary [↓]
- (2) ϕ , the avg # of pathlets that represent each trajectory [↓]
- (3) L_{traj} , the # of trajectories discarded (expressed in %) [↓]
- (4) $\bar{\mu}$, the average representability across the remaining trajectories (expressed in %) [↑]

Note that the third and fourth metrics above do not apply to Chen et al.’s [8] and Agarwal et al.’s [1] methods as such measures are only applicable to pathlet-merging methods. Moreover, the fourth metric does not apply to PATHLETRL-NR. Under this model, all remaining trajectories in the dataset (and hence the average) are always 100% representable, which is not so interesting.

4.5 Results and Discussion

In this section, we go over each of the six research questions, present the experimental results and provide some discussion.

(Q1) Quality of the Extracted PDs. We evaluate the pathlet dictionary extracted by our PATHLETRL algorithm against the PDs extracted by SOTA baselines. See Table 5 for the numerical results, where

		Baselines		NULL	PATHLETRL			
		[8]	[1]	SGT	RND	NR	UNW	(OURS)
TORONTO	$\lfloor \downarrow \rfloor \mathcal{S} $	13,886	7,982	2,563	2,454	1,896	<u>1,801</u>	1,743
	$\lfloor \downarrow \rfloor \phi$	7.02	5.97	4.76	3.77	2.89	3.98	3.75
	$\lfloor \downarrow \rfloor L_{traj}$	N/A	N/A	0%	19.7%	17.6%	15.1%	<u>15.2%</u>
	$\lfloor \uparrow \rfloor \bar{\mu}$	N/A	N/A	100%	79.9%	N/A	<u>80.0%</u>	80.0%
ROME	$\lfloor \downarrow \rfloor \mathcal{S} $	59,396	31,017	15,465	9,718	7,003	5,804	5,291
	$\lfloor \downarrow \rfloor \phi$	202.91	188.33	230.15	173.04	158.18	<u>146.39</u>	139.89
	$\lfloor \downarrow \rfloor L_{traj}$	N/A	N/A	0%	24.9%	<u>21.1%</u>	22.9%	20.4%
	$\lfloor \uparrow \rfloor \bar{\mu}$	N/A	N/A	100%	82.7%	N/A	86.2%	<u>85.6%</u>

Table 5. Numerical results showing the attributes of the pathlet dictionaries extracted by each method for each dataset.

the bold numbers indicate the result of the most superior model for the given PD metric and the underlined number is the result of the second-best performing model (note that we do not boldface or underline the numbers of SGT as such model serves as the null model where nothing is done to the pathlet graph). Although the nature of the pathlet definition and the approaches are not necessarily the same, the algorithms of Chen et al. [8] and Agarwal et al. [1] are still comparable. We ultimately show that their top-down approaches are not as effective as our bottom-up strategies. First, we look at the size of the pathlet dictionary, $|\mathcal{S}|$, where the smaller the number the better is the result. Our PATHLETRL model was able to improve from SGT by $\sim 32.0\%$ ($\sim 65.8\%$) for the TORONTO (ROME) dataset. These numbers are an $\sim 87.4\%$ ($\sim 91.1\%$) improvement from Chen et al.’s [8] model on the TORONTO (ROME) dataset. Our model also improves by $\sim 78.2\%$ ($\sim 82.9\%$) from Agarwal et al.’s [1] method on the TORONTO (ROME) dataset. These two observations indicate how superior our method is against the state-of-the-art; i.e., bottom-up methods being better than top-down schemes. Note as well that Chen et al.’s [8] and Agarwal et al.’s [1] PDs are larger than the initial # of length-1 pathlets, as their methods are top-down – which initially considers all possible pathlet sizes and configurations (including overlaps). Clearly, they do not exhibit ideal results, compared to our proposed PATHLETRL model, as well as in all of the ablation versions of PATHLETRL.

Then, we focus on the metric of the average pathlet number that represents each trajectory (which can go up or down at each step of the iterative algorithm). Similar to $|\mathcal{S}|$, a smaller ϕ indicates a more ideal dictionary. Our PATHLETRL model was able to extract dictionaries that improve from SGT by $\sim 21.2\%$ ($\sim 39.2\%$) on the TORONTO (ROME) dataset. Meanwhile, Chen et al.’s [8] PD has ϕ quality $\sim 47.4\%$ higher than SGT for TORONTO dataset, and only $\sim 11.8\%$ lower than SGT on ROME dataset. A similar trend can be seen in Agarwal et al.’s [1] dictionary, with $\sim 25.4\%$ higher and $\sim 18.2\%$ lower than the initial number in the TORONTO and ROME datasets respectively. Clearly, our proposed PATHLETRL (and its ablation variations) outperforms these SOTA baselines.

Our PATHLETRL also improves from SGT based on the $|\mathcal{S}|$ and ϕ metrics. Because no action is taken on the pathlet graph in SGT, only the original numbers are shown; thus, L_{traj} and $\bar{\mu}$ remains as 0% and 100% for both datasets. However, we can see the benefits of PATHLETRL by trading off these values to obtain smaller dictionaries with much less ϕ scores – as controlled by the α parameters.

(Q2) Memory Efficiency. Fig. 2 (in log scale) demonstrates how much more memory-efficient PATHLETRL is compared to the baselines [1, 8]. As can be seen in Fig. 2, our method gets as input a set of trajectories that requires ~ 900 MB ($\sim 30+$ GB) to be stored in memory, and builds a trajectory pathlet dictionary that requires a mere ~ 100 KB (~ 1 MB) for the TORONTO (ROME) dataset. In fact,

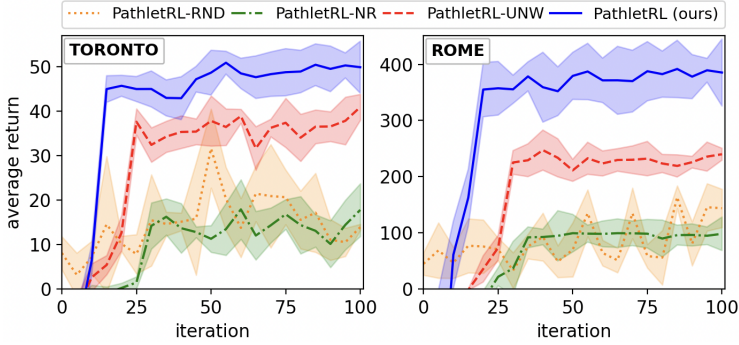


Fig. 7. Performance evaluation of proposed and ablation PATHLET-RL models, measured using the average return metric of $m = 5$ episodes across $n = 100$ iterations (run 10 times)

this represents a $\sim 7.4K\times$ ($\sim 24K\times$) saving. This considerable improvement can be attributed to the fact that our method uses a bottom-up approach where only edge-disjoint pathlets are considered. In contrast, the current baselines follow a top-down approach, where the trajectory pathlet dictionary consists of overlapping pathlets of various sizes and configurations, most of which are redundant.

(Q3) Ablation Study. Next, we perform an ablation experiment to see how well our proposed PATHLET-RL model performs. Fig. 7 displays the average returns of PATHLET-RL and its ablations across n iterations on the two datasets. We can observe similar trends on both datasets. Notice that PATHLET-RL-RND has the poorest performance, exhibiting a random RL policy that shows no learning at all. Meanwhile, all other models demonstrate that their average return value converges after some iterations (for example, 15 and 20 iterations for PATHLET-RL on the TORONTO and ROME datasets), and then fluctuating slightly within a small range. PATHLET-RL-NR, while it demonstrates some level of learning due to the DQN policy, does not perform well compared to PATHLET-RL-UNW – which suggests that representability is an essential component. This unweighted version of PATHLET-RL can be seen as a runner up to our (weighted) proposed model, which indicates that there is some value to assigning pathlet weights than simply weighing all pathlets equally.

Besides comparing the trends of PATHLET-RL models’ performance evaluation, we can also look at the quality of their PDs (see Table 5 for the results). Generally speaking, our proposed PATHLET-RL’s PD is superior than the PDs extracted by its ablation variations (i.e., the $|\mathcal{S}|$ metrics for both the TORONTO and ROME datasets, the $\bar{\mu}$ metric for the TORONTO dataset, and the ϕ and L_{traj} metrics for the ROME dataset). In other cases that PATHLET-RL did not rank first, it was a runner up but this can be explained. For instance, consider the ϕ metric in the TORONTO dataset. The reason for the higher quality of PATHLET-RL-NR’s PD than that of PATHLET-RL’s in terms of the ϕ metric is that because trajectory counts easily shrink faster in PATHLET-RL-NR; the average ϕ can easily go down should the number of pathlets representing each trajectory also dwindle in number. The $\bar{\mu}$ metric for the PD of PATHLET-RL-UNW is higher than that of the PD of PATHLET-RL on the ROME dataset, which could be because PATHLET-RL-UNW has fewer trajectories remaining in its trajectory set and that it just so happened that those that remained have high representability μ values. Regardless, the differences in numbers between the PDs of PATHLET-RL and PATHLET-RL-UNW in terms of the $\bar{\mu}$ metric is small and still comparable. The same can be said for the L_{traj} metric of the PDs of PATHLET-RL-UNW and PATHLET-RL on the TORONTO dataset, which differs by only a measly $\sim 0.1\%$ – demonstrating that PATHLET-RL is still competitive.

(Q4) Pathlet Length Distribution. We also analyze the length distribution of the pathlets in our dictionaries. The trend is similar for both datasets (Fig. 8 shows the pathlet length distribution, with the y -axis in log scale). The PATHLET-RL-RND has a decreasing # for longer pathlets, which

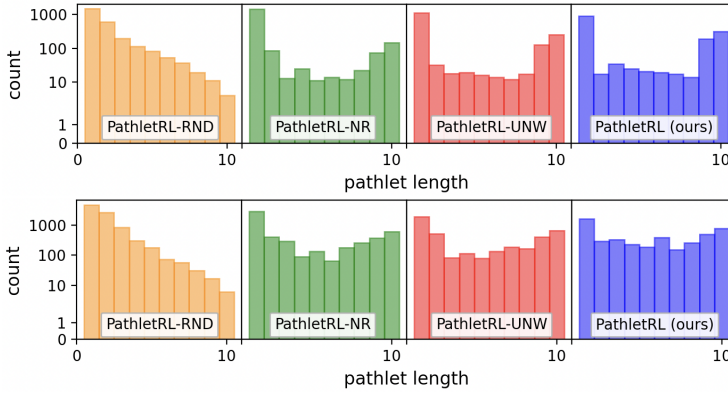


Fig. 8. The pathlet length distribution of pathlet dictionaries obtained by PATHLETRL model and its ablation versions on the TORONTO (top) and ROME (bottom) datasets.

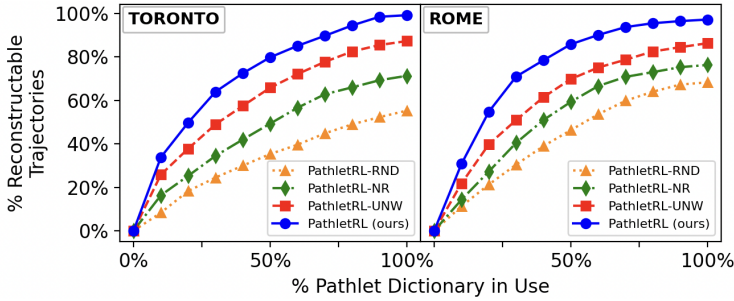


Fig. 9. The % of evaluation trajectories reconstructable from a sample set taken from extracted pathlet dictionaries.

is intuitive as the random policy blindly keeps & merges pathlets. It is harder to maintain longer pathlets in this random probabilistic manner as pathlets that terminate their growth are already considered “processed” and cannot grow further. As a result, it is more rare to see higher-ordered pathlets than shorter pathlets in PATHLETRL-RND’s PD. The rest of the other RL models utilizing DQN policy have longer-length pathlets as expected (with more length-9 and 10 pathlets in the dictionary). Our proposed PD can capture more of these higher-ordered pathlets – indicating a smaller pathlet dictionary, as reflected by the results in Table 5. Meanwhile, we can still observe a large number of length-1 pathlets, which may be due to a number of reasons. One could be that some of the length-1 pathlets are still *unprocessed* (as a result of early stopping caused by the various termination criteria in our algorithm). It could also be that some of the length-1 processed pathlets are unmerged due to the algorithm’s recommendation based on the utility, or perhaps based on pathlets losing all neighbor pathlets to merge with. The latter case depicts a scenario for where a length-1 processed pathlet ρ may have lost all its neighbor pathlets as a result of these neighbors merging amongst one another, leaving no way for ρ to merge with any of these formed merged pathlets.

(Q5) Partial Trajectory Reconstruction. See Fig. 9 for a plot that displays the results of this experiment, where we determine how much of the dictionary is adequate enough to reconstruct most of our trajectories in our testing set. Here, we say that a trajectory is *reconstructable* if its representability value $\mu \geq 0.75$ (i.e., 75% of the trajectory can be represented by the PD). Anything less would mean that the trajectory is not reconstructable due to an excessive number of gaps. Ideally, we would like to take the top $x\%$ of the pathlets in the PD that are the most traversed by

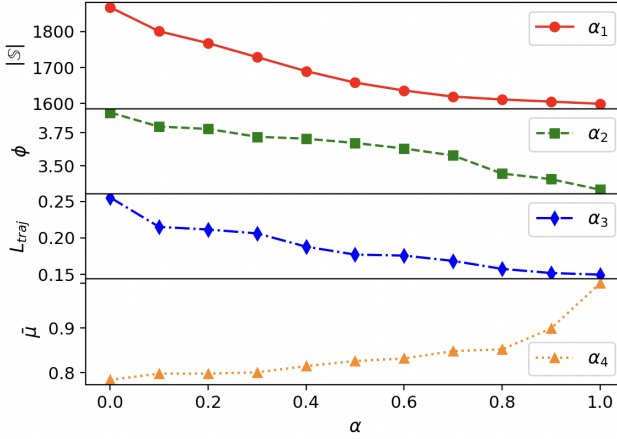
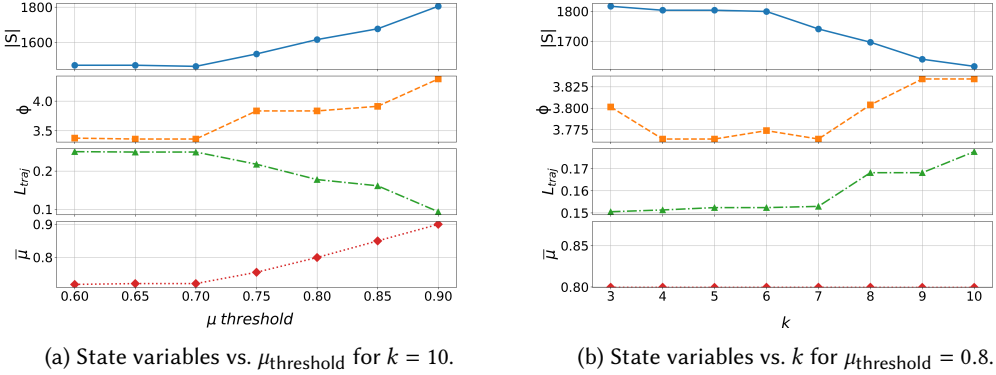


Fig. 10. Parameter sensitivity experiment: the impact of α 's on the quality of PATHLETRL's pathlet dictionary the trajectories in the training set. However, we can further remove the bias in the experiment by choosing instead a random sample of $x \in [10\%, 20\%, \dots, 100\%]$ pathlets in the extracted PD, and measuring how much of the trajectories in the testing set are reconstructable by this pathlet sample set. As shown in the results, by using around half of the pathlets in PATHLETRL's PD, a good $\sim 80\%$ ($\sim 85\%$) of the trajectories in the TORONTO (ROME) testing set can be reconstructed; and by using the whole dictionary, almost all trajectories in the set can be reconstructed. This shows that our proposed model is able to extract a high-quality pathlet dictionary. Comparing this with our ablation versions, they all follow a similar trend for both datasets – i.e., the amount of trajectories that the dictionaries of the ablation models can reconstruct is less than the amount that our proposed PATHLETRL's dictionary can do so. The worst being is PATHLETRL-RND's dictionary that can reconstruct up to only $\sim 50\%$ ($\sim 65\%$) of the trajectories in TORONTO (ROME) given the entire dictionary.

(Q6) Parameter Sensitivity Analysis. We then discuss how the values of the four α values ($\alpha_1, \alpha_2, \alpha_3, \alpha_4$) affect the output PD's quality in terms of its four attributes: $|\mathbb{S}|, \phi, L_{traj}, \bar{\mu}$ respectively⁸. There are four stacked plots, as seen in Fig. 10. The first one depicts the changes to the PD's $|\mathbb{S}|$ as we vary $\alpha_1 = [0.0, 0.1, \dots, 1.0]$ (while keeping the other α terms equal $\alpha_2 = \alpha_3 = \alpha_4 = \frac{1-\alpha_1}{3}$). We notice, as expected, a decreasing trend; larger α_1 values indicate higher importance to a smaller dictionary size. By varying α_2 and keeping the other terms equal, we can also observe a decreasing trend; higher α_2 values imply a stronger emphasis on lower ϕ scores – that is, lower average number of pathlets representing trajectories. Then when term α_3 's value is varied, while keeping other α terms the same, it also shows a trend that decreases as we increases α_3 . The greater the α_3 is, the more importance we put into keeping the trajectory loss low. Finally, varying α_4 while keeping the other α terms equal, shows an opposite trend than the other α terms. Here, we can observe that larger α_4 values are indicative of greater importance towards possessing higher representability values.

(Q7) Hyper-Parameter Impact on Model Performance. We analyze the impact of the hyper-parameters $\mu_{\text{threshold}}$ and k on the attributes $|\mathbb{S}|, \phi, L_{traj}$, and $\bar{\mu}$. When varying $\mu_{\text{threshold}}$ with a fixed $k = 10$, we observe several trends. The size of the set ($|\mathbb{S}|$) remains stable at first but grows substantially as $\mu_{\text{threshold}}$ increases, indicating that, as anticipated, higher values of $\mu_{\text{threshold}}$ lead to larger pathlet counts. This is because the episodes become shorter as we the agent hits the

⁸**Note:** the goal here is not to find an optimal value for α_i , but intends on showing the trend of how $|\mathbb{S}|, \phi, L_{traj}, \bar{\mu}$ changes with varying values of $\alpha_1, \alpha_2, \alpha_3, \alpha_4$ respectively.

(a) State variables vs. $\mu_{\text{threshold}}$ for $k = 10$.(b) State variables vs. k for $\mu_{\text{threshold}} = 0.8$.Fig. 11. Comparison of state variables under varying $\mu_{\text{threshold}}$ and k hyper-parameters.

threshold more quickly. The average number of pathlets per trajectory (ϕ) remains relatively constant at lower thresholds but increases when $\mu_{\text{threshold}}$ is higher, indicating that more pathlets are required to represent each trajectory since fewer merges occur as the threshold is reached sooner. The relationship between the Trajectory Loss (L_{traj}) and the Average Representability ($\bar{\mu}$) exhibits opposing trends as the values of $\mu_{\text{threshold}}$ increase. This is because when $\mu_{\text{threshold}}$ is set below a certain value (70% in this case), the trajectory loss threshold (set at 25%) becomes the determining factor for termination, as it is reached before the lower $\mu_{\text{threshold}}$. However, when $\mu_{\text{threshold}}$ exceeds 70%, $\bar{\mu}$ matches the $\mu_{\text{threshold}}$ because it now becomes the primary terminating criterion. As a result, the trajectory loss no longer dictates termination and begins to decrease, since fewer pathlets are merged, leading to a lower number of lost trajectories.

When fixing $\mu_{\text{threshold}} = 0.8$ and varying k , a distinct set of trends emerges. The size of the set ($|\mathcal{S}|$) decreases as k increases, suggesting that using longer pathlets results in a more compact PD, as anticipated. The average number of pathlets per trajectory (ϕ) shows a slight increase with higher k , indicating that trajectories are broken into more segments as k rises. The trajectory loss (L_{traj}) increases as expected, reflecting a minor reduction in reconstruction quality as more pathlets are merged together. Additionally, the $\mu_{\text{threshold}}$ remains fixed at 80%, consistent with the initial parameter setting mentioned earlier.

We analyze the distribution of pathlet lengths generated for various values of k and a fixed $\mu_{\text{threshold}}$. It is evident that increasing the maximum pathlet length (k) encourages the agent to merge more pathlets, thereby reducing the number of pathlets with an initial length of 1. Furthermore, the plots reveal that although pathlets of varying lengths are present in each setting, the agent predominantly generates pathlets that are close to the maximum length k , rather than distributing them evenly across lengths from 1 to k . When examining the effect of different $\mu_{\text{threshold}}$ values, we see that lower $\mu_{\text{threshold}}$ values allow for greater merging, resulting in a higher proportion of merged pathlets, as expected.

5 PATHLETRL OPTIMIZATIONS

Building on the parameter sensitivity analysis, which showed how variations in the four α parameters influence the Pathlet Dictionary (PD) in terms of the different objectives, we now shift our focus to addressing the observed limitations in the original PATHLETRL model. Specifically, the analysis highlighted the model's sensitivity to the weight assignments in the linear scalarization of the reward function, which can significantly impact the quality of the extracted PD.

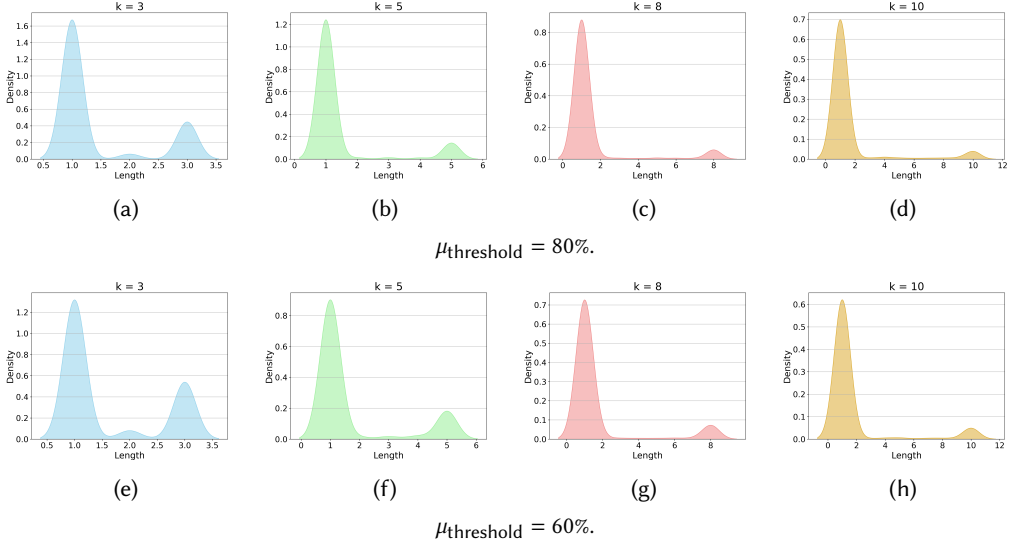


Fig. 12. Comparison of pathlet length distributions for different values of k under two different $\mu_{\text{threshold}}$ settings (80% and 60%) using Kernel Density Estimation.

To mitigate this sensitivity and further enhance the model’s performance, we propose three variations of the PATHLETRL framework. The first two variations introduce alternative scalarization techniques to better balance the competing objectives: (1) PATHLETRL with Chebyshev Scalarization (PATHLETRL_{Cheb}) and (2) PATHLETRL with a Custom Dynamic Scalarization Function (PATHLETRL_{DS}). The third variation, PATHLETRL++, extends PATHLETRL_{DS} by incorporating a richer state representation. This enhancement provides the reinforcement learning agent with a more detailed and informative view of the environment, enabling more nuanced decision-making and ultimately leading to improved performance in reducing the size of the candidate pathlet set.

5.1 Scalarization Sensitivity in Multi-Objective Optimization

The original PATHLETRL model employs a linear scalarization approach for reward calculation, equally weighting all of the objectives (3). This linear scalarization suffers from known sensitivity issues in multi-objective optimization (MOO), as small changes in weight assignment can lead to substantially different optimization outcomes [47]. Specifically, Linear scalarization only guarantees optimal solutions when the Pareto front (the set of optimal trade-offs between objectives) is convex. If the Pareto front is non-convex, this method fails to identify non-convex Pareto optimal solutions. This limitation means that some potentially desirable trade-offs between objectives may be missed entirely [19]. To address these issues, we propose two alternative scalarization methods to improve the stability and generalization of solutions.

5.1.1 Chebyshev Scalarization. The first alternative is Chebyshev scalarization, which seeks to minimize the maximum deviation from the ideal point in the objective space. This approach is formally expressed as:

$$R_{\text{Chebyshev}} = -\max(\alpha_1 |f_1(\mathbf{x}) - z_1^*|, \alpha_2 |f_2(\mathbf{x}) - z_2^*|, \alpha_3 |f_3(\mathbf{x}) - z_3^*|, \alpha_4 |f_4(\mathbf{x}) - z_4^*|), \quad (4)$$

where \mathbf{x} represents the decision variables, $f_1(\mathbf{x})$, $f_2(\mathbf{x})$, $f_3(\mathbf{x})$, $f_4(\mathbf{x})$ are the values of the four objective functions, and z_1^* , z_2^* , z_3^* , z_4^* are the ideal values of the respective objectives. The weights α_1 , α_2 , α_3 , α_4 are user-defined scaling factors, often set such that $\sum_{i=1}^4 \alpha_i = 1$.

Chebyshev scalarization does not depend heavily on weight allocations and can find Pareto-optimal solutions in both convex and non-convex regions of the Pareto front [47]. It ensures balanced optimization across all objectives and leads to robust solutions.

5.1.2 Dynamic Scalarization. The second alternative introduces a dynamic scalarization function that adjusts weights based on the agent's proximity to predefined thresholds for trajectory representability μ_{traj} and trajectory loss L_{traj} . This method is captured by dynamically adjusting the weights for different objectives using penalties. These penalties are calculated based on the agent's proximity to critical thresholds.

The dynamic weight assignment is implemented in the following way:

$$w_{\text{traj}}(t) = \frac{1}{\max\left(0.01, \frac{M - L_{\text{traj}}(t)}{M}\right)}$$

$$w_{\mu}(t) = \frac{1}{\max\left(0.01, \frac{\mu_{\text{traj}}(t) - \tau_{\mu}}{0.2}\right)}$$

where $w_{\text{traj}}(t)$ and $w_{\mu}(t)$ are dynamic weights for trajectory loss and trajectory representability, respectively. The weight for each objective increases as the agent approaches the thresholds τ_{μ} for μ_{traj} and M for L_{traj} , encouraging the agent to prioritize these objectives when performance is critical.

The reward is calculated using these dynamic weights:

$$R = -\alpha_1 \Delta |S| - \alpha_2 \Delta \phi - \alpha_3 \Delta L_{\text{traj}} w_{\text{traj}}(t) + \alpha_4 \Delta \bar{\mu} w_{\mu}(t), \quad (5)$$

Initially, all objectives are weighted equally, but as the agent approaches critical thresholds (e.g., the trajectory representability threshold $\tau_{\mu_{\text{traj}}}$), the dynamic weights $w_{\text{traj}}(t)$ and $w_{\mu}(t)$ increase, forcing the agent to prioritize those objectives more.

At the end of an episode, an additional reward or penalty is applied based on how well the agent performed overall, considering the same objectives and thresholds. This dynamic adjustment ensures that the agent becomes more conservative when nearing critical thresholds, avoiding excessive pathlet merging that could degrade the overall performance.

5.2 Enhanced State Representation for Improved Decision-Making

While the first two variations improve the scalarization mechanism, they still rely on the original state representation used by PATHLETRL, which is limited to global metrics such as pathlet count, average trajectory representability, and trajectory loss. The state at time t is represented as:

$$\mathbf{s}_t = (S_1, S_2, S_3, S_4),$$

where S_1 denotes the number of pathlets in the current pathlet graph, S_2 denotes the average number of pathlets required to represent the trajectories, S_3 is the trajectory loss, and S_4 is the average trajectory representability. This restricted global view leaves the reinforcement learning agent unaware of crucial local information about individual pathlets and their neighbors, which can lead to suboptimal decision-making, especially when determining which pathlets to merge or split.

To address this shortcoming, we propose a third variation: PATHLETRL++. This model extends the dynamic scalarization method by incorporating a more detailed state representation, which provides the agent with weights of both the current pathlet and its neighboring pathlets. This

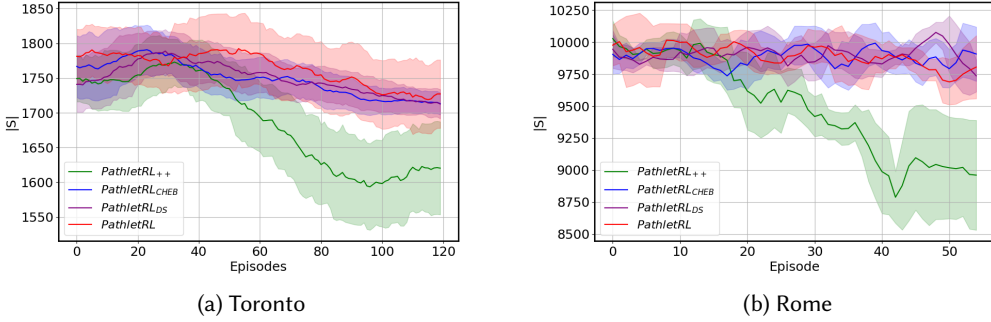


Fig. 13. Training performance of different PATHLETRL variations on the Toronto and Rome datasets.

enriched representation gives the agent a better view of its environment, enabling more informed and precise decisions during pathlet merging.

5.2.1 Local Metrics for Improved State Representation. The enhanced state representation at time t , denoted as s_t^{enhanced} , is extended to include both global metrics and local pathlet weights. Specifically, the state is now formulated as:

$$s_t^{\text{enhanced}} = (S_1, S_2, S_3, S_4, w_t, w_t^{\text{neighbors}}),$$

where:

- w_t represents the weight of the pathlet selected for processing at time t (p_{current}).
- $w_t^{\text{neighbors}}$ denotes the weights of the selected pathlet's neighbours:

$$w_t^{\text{neighbors}} = (w_p) \quad \forall p \in \mathcal{N}(p_{\text{current}}),$$

where $\mathcal{N}(p_{\text{current}})$ represents the set of neighboring pathlets to p_{current} .

5.3 Comparative Analysis

To maintain evaluation consistency, all models were tested using the same Toronto map and trajectory dataset. Additionally, we utilized a modified version of the Rome dataset to challenge the models with a larger set of trajectories. Typically, taxi cabs send GPS signals every 15 seconds. In our modification, the trajectory data were map matched using a shorter separation time frame of 60 seconds—if a taxi did not send a signal for over a minute, its path was considered a new trajectory. This approach resulted in a significantly larger number of trajectories (75,180).

5.3.1 Training Performance Analysis. To better understand the training dynamics of the proposed variations, we analyze the evolution of pathlet dictionary size with respect to the number of training episodes. Figures 13a and 13b show the pathlet size reduction over the training episodes for each model variant on the Toronto and Rome datasets, respectively.

Focusing first on the Toronto dataset, it is evident that all models demonstrate a downward trend in pathlet size, indicating their learning to minimize the dictionary size effectively before reaching predefined thresholds. Notably, PATHLETRL++ converges to a smaller pathlet dictionary size more rapidly than the other models. This swift convergence highlights the model's enhanced training efficiency, which can be attributed to its detailed observation of the environment and robust reward system.

In contrast, when analyzing the Rome dataset, the original PATHLETRL variants with the standard state space representation encounter difficulties in learning meaningful actions due to the large

		PATHLETRL VARIATIONS			
		PATHLETRL	PATHLETRL _{CHEB}	PATHLETRL _{DS}	PATHLETRL++
TORONTO	[↓] \mathbb{S}	1762	1736	1735	1646
	[↓] ϕ	3.78	3.77	3.76	3.86
	[↓] L_{traj}	15.8%	16.6%	16.4%	17.4%
	[↑] $\bar{\mu}$	80.0%	80.0%	80.0%	80.0%
ROME	[↓] \mathbb{S}	9811	9871	9801	9068
	[↓] ϕ	19.76	19.68	19.69	19.84
	[↓] L_{traj}	1.8%	1.8%	1.8%	1.9%
	[↑] $\bar{\mu}$	80.0%	80.0%	80.0%	80.0%

Table 6. Performance Comparison of PathletRL Variations on Toronto and Rome Datasets.

number of trajectories. Despite this challenge, PATHLETRL++ again demonstrates a rapid learning rate and achieves a substantial reduction in pathlet size.

Overall, it is clear that integrating local pathlet metrics within PATHLETRL++ not only enhances the final performance but also accelerates the training process. This results in more optimal solutions being reached in fewer training episodes.

5.3.2 Offline Performance Comparison. Table 6 summarizes the performance of the original PATHLETRL model and its variants across the four key metrics on both the Toronto and Rome datasets. For the Toronto dataset, PATHLETRL++ achieves the smallest pathlet dictionary size $|\mathbb{S}|$, comprising only 1,646 pathlets, which is notably lower than the 1,762 pathlets used by the original PATHLETRL model. When considering the average number of pathlets representing each trajectory (ϕ), the results are relatively similar across models, with PATHLETRL_{DS} showing a slight advantage. In terms of trajectory loss (L_{traj}), the original PATHLETRL model performs best with a loss rate of 15.8%. This outcome is expected since its larger pathlet dictionary size results in fewer trajectory merges, minimizing loss. All models maintain the same average representability ($\bar{\mu}$) of 80.0% which is equal to the μ threshold that we set for the training.

On the more complex Rome dataset, PATHLETRL++ again demonstrates superior performance by achieving a smaller pathlet dictionary size of 9,068 compared to over 9,800 for the other models. This indicates its scalability and efficiency when handling larger datasets. Similar to the Toronto results, the average number of pathlets per trajectory (ϕ) remains comparable across models, with PATHLETRL_{CHEB} achieving the lowest value. The trajectory loss (L_{traj}) is nearly identical across all models, ranging from 1.8% to 1.9%, reflecting the large volume of trajectories in the Rome dataset. Once again, all models maintain the same average representability ($\bar{\mu}$) of 80.0%, consistent with the training threshold.

Although PATHLETRL++ marginally increases the trajectory loss compared to the original PATHLETRL model on both datasets, this is offset by its ability to reduce the pathlet dictionary size more significantly. This reduction in pathlet size can lead to improved scalability and computational efficiency, making PATHLETRL++ a preferable choice for larger datasets or scenarios.

6 RELATED WORK

Our research is related to (i) *trajectory data mining*, (ii) *pathlet mining*, (iii) *subtrajectory clustering*, and (iv) *deep learning for spatiotemporal data*. We cover below some of the most significant efforts relevant to our work. Note that some related works have already been cited throughout the manuscript to maintain a focused discussion, so they are largely omitted in this section.

6.1 Trajectory Data Mining

Trajectory data mining has been an active research direction for a long time [6, 16, 62]. This high interest can largely be attributed to the rapid development and prominence of geospatial technologies [11], location-based smart devices [40], abundance of GPS-based applications [37], and generation of massive trajectory datasets [13]. The focus is on popular technical problems, including trajectory similarity [12] and trajectory clustering [17]. Modeling trajectory data using graphs to address complex trajectory mining tasks has also been a popular approach in recent years. Example tasks include, but are not limited to similarity search [12], recovery [10], node centrality computation [39], mining spatiotemporal interactions [42, 43], learning semantic relationships of geographic areas [29] and recommendations [48, 53].

6.2 Pathlet Mining

Pathlet mining focuses on discovering patterns and extracting knowledge by decomposing complex trajectories into a set of fundamental building blocks known as pathlets. These pathlets serve as essential units that can efficiently represent a wide range of trajectories, aiding in tasks such as trajectory compression, classification, and route planning.

One of the pioneering works in this area is by Chen et al. [8], who introduced the concept of a pathlet dictionary for compressing and planning trajectories. Their goal was to capture shared spatial and temporal regularities among a collection of human trajectories by learning a set of common path segments, or pathlets, that can be concatenated to reconstruct the original trajectories. They formulated the problem as an integer linear programming (ILP) task, aiming to minimize both the size of the pathlet dictionary and the number of pathlets required to represent each trajectory. To address the computational challenges of solving the ILP on large datasets, Chen et al. [8] proposed an efficient decoupled approach that optimizes a lower bound of the original objective function. This method scales linearly with the number of trajectories, making it practical for large-scale applications. Their approach allows for the extraction of meaningful pathlets that reflect common movement patterns within the data. The learned pathlet dictionary can be utilized in various applications, such as route planning and trajectory analysis, by enabling efficient reconstruction and representation of trajectories.

Zhou et al. [63] proposed the bag of segments method to represent motion trajectories. Inspired by the “bag of words” model from text mining, their method represents each trajectory as a collection of segments assigned to codewords from a predefined dictionary. This approach transforms trajectories into vectors in the codeword space, enabling the use of traditional machine learning algorithms for trajectory classification and similarity search. While both Chen et al. [8] and Zhou et al. [63] focus on representing trajectories using fundamental building blocks, their methodologies differ. Chen et al. [8] emphasize trajectory compression and shared pattern extraction through an optimization framework aimed at minimizing the pathlet dictionary size and reconstruction cost. Zhou et al. [63], on the other hand, focus on transforming trajectories into a vector space representation using clustering techniques, facilitating trajectory analysis tasks.

Other notable contributions to the field include the work by Panagiotakis et al. [36], who developed a method for identifying representative subtrajectories using global voting, segmentation, and sampling techniques. Their approach enhances trajectory summarization and pattern discovery by focusing on the most representative segments within a dataset. Additionally, Wang et al. [51] addressed the problem of finding the top k representative routes that cover as many trajectories as possible under budget constraints and distance thresholds. They proposed three near-optimal solutions that efficiently solve this problem, offering valuable strategies for trajectory analysis under resource limitations.

However, these top-down approaches often face challenges related to high memory usage and redundant storage due to overlapping pathlets, as they generate a large number of candidate pathlets and select a subset for the dictionary. To address these limitations, we propose a bottom-up strategy that incrementally merges basic pathlets to build a compact and efficient pathlet dictionary. Our approach begins with unit-length pathlets and iteratively merges them while optimizing utility, defined using newly introduced metrics of trajectory loss and representability. By utilizing a deep reinforcement learning framework, specifically Deep Q-Networks (DQN), the method approximates the utility function and results in significant reductions in memory requirements—up to 24,000 times compared to baseline methods.

6.3 Subtrajectory Clustering

Pathlet mining is commonly framed as a subtrajectory clustering problem. Lee et al. [22] proposed the TRACULUS algorithm, which partitions trajectories into line segments and then groups those segments that lie in similar dense regions to form clusters. This approach effectively captures frequently traversed paths by clustering spatially close trajectory segments.

Van Kreveld et al. [46] designed a novel measure for mining median trajectories, serving as cluster centroids of (sub)trajectories. Their method focuses on discovering well-visited routes by identifying median paths that represent common movement patterns within a set of trajectories.

Agarwal et al. [1] advanced the field by introducing a comprehensive model for subtrajectory clustering using the concept of a pathlet cover. Inspired by the classical set cover problem, their method aims to find a small set of pathlets that effectively represent the shared portions of trajectories in a dataset. In their model, each trajectory is considered as a concatenation of a small set of pathlets, allowing for possible gaps to account for unique segments or noise. They formulated the subtrajectory clustering problem with a single objective function that balances three key factors: minimizing the number of pathlets selected, ensuring high-quality representation of subtrajectories by the pathlets (by minimizing the distance between subtrajectories and their assigned pathlets), and penalizing the presence of gaps in trajectories. Recognizing the NP-hardness of the problem, Agarwal et al. [1] developed efficient approximation algorithms with provable guarantees on solution quality and running time. Their approach leverages geometric properties of trajectories and employs strategies like greedy selection and geometric grouping to efficiently explore the space of possible pathlets without exhaustive enumeration. In all these subtrajectory clustering methods, the cluster centroids are seen as popular segments traversed by many trajectories and can alternatively be viewed as pathlets. This perspective facilitates the discovery of shared movement patterns and supports applications such as trajectory summarization, anomaly detection, and efficient data compression.

6.4 Deep Learning for Spatiotemporal Data

In recent years, deep learning methods have been proposed for learning representations of spatiotemporal data [50]. Chen et al. [9], for instance, introduced a comprehensive review of deep learning applications for trajectory data management and mining. This work highlights the use of advanced AI techniques for various tasks like trajectory prediction, clustering, and anomaly detection. A key contribution is the provision of an open-source repository of trajectory-related datasets, enabling researchers to access curated resources for diverse mobility analysis tasks. Moreover, a diffusion model, TrajGDM, was developed to simulate human mobility patterns, allowing more sophisticated generation of trajectory data based on real-world movement behaviors [64]. These advancements indicate the growing adoption of generative models in trajectory mining. Other works explore spatiotemporal reachability and the use of graph neural networks (GNNs) to mine complex relationships from trajectory data [61]. Recent work, such as Traj-LLM (Lan et al.

[21]), explores the use of Large Language Models (LLMs) in trajectory prediction tasks, leveraging their ability to capture complex traffic semantics and scene understanding to enhance prediction accuracy and adaptability. Of particular interest are deep reinforcement learning based methods that are often evaluated on agents playing a specific game [45]. These methods have successfully been adapted and shown promise in addressing several complex trajectory-related problems, such as route planning [15], trajectory simplification [52], and adaptive vehicle navigation problem [5].

7 CONCLUSIONS

Constructing trajectory pathlet dictionaries—small sets of building blocks capable of representing large numbers of trajectories—has become crucial due to applications in route planning, travel time estimation, and trajectory compression. This work introduces a deep reinforcement learning solution, PATHLETRL, which generates a dictionary 65.8% smaller than traditional methods. Remarkably, only half of the pathlets in PATHLETRL’s dictionary are needed to reconstruct 85% of the original trajectory dataset, whereas baselines require their entire dictionaries to reconstruct just 65% of the trajectories. Additionally, PATHLETRL achieves significant memory savings—up to $\sim 24,000\times$ compared to existing methods—due to reduced initial memory requirements for storing pathlets. To further enhance PATHLETRL, we proposed three new variations to address its reward function limitations and to incorporate richer and more meaningful state representations. These improvements led to a more compact dictionary, faster convergence, and better overall performance in terms of dictionary size and training efficiency, making PATHLETRL++ the best-performing variant for large-scale trajectory datasets.

REFERENCES

- [1] Pankaj K. Agarwal, Kyle Fox, Kamesh Munagala, Abhinandan Nath, Jiangwei Pan, and Erin Taylor. 2018. Subtrajectory Clustering: Models and Algorithms. In *Proc. of the 37th ACM SIGMOD-SIGACT-SIGAI Symposium on Principles of Database Sys. (PODS '18)*. 75–87.
- [2] Fuad Aleskerov, Denis Bouyssou, and Bernard Monjardet. 2007. *Utility Maximization, Choice and Preference*. Springer Berlin Heidelberg, Berlin, Heidelberg.
- [3] Gian Alix, Nina Yanin, Tilemachos Pechlivanoglou, Jing Li, Farzaneh Heidari, and Manos Papagelis. 2022. A Mobility-based Recommendation System for Mitigating the Risk of Infection during Epidemics. In *2022 23rd IEEE Intl. Conf. on Mobile Data Mgt. (MDM)*. 292–5.
- [4] Mahmoud Alsaeed, Ameeta Agrawal, and Manos Papagelis. 2023. Trajectory-User Linking using Higher-order Mobility Flow Representations. In *2023 24th IEEE International Conference on Mobile Data Management (MDM)*. 158–167.
- [5] Fazel Arasteh, Soroush SheikhGarGar, and Manos Papagelis. 2022. Network-Aware Multi-Agent Reinforcement Learning for the Vehicle Navigation Problem. In *Proc. of the 30th Intl. Conf. on Adv. in Geographic Info. Sys. (ACM SIGSPATIAL '22)*. Article 69.
- [6] Gowtham Atluri, Anuj Karpatne, and Vipin Kumar. 2018. Spatio-Temporal Data Mining: A Survey of Problems and Methods. *ACM Comp. Surveys* 51, 4, Article 83 (Aug 2018).
- [7] Lorenzo Bracciale, Marco Bonola, Pierpaolo Loreti, Giuseppe Bianchi, Raul Amici, and Antonello Rabuffi. 2014. CRAWDAD Roma/taxi dataset. <https://crawdad.org/roma/taxi/20140717>.
- [8] Chen Chen, Hao Su, Qixing Huang, Lin Zhang, and Leonidas Guibas. 2013. Pathlet Learning for Compressing and Planning Trajectories. In *Proc. of the 21st ACM SIGSPATIAL Intl. Conf. on Adv. in Geographic Info. Sys. (ACM SIGSPATIAL '13)*. 392–5.
- [9] Wei Chen, Yuxuan Liang, Yuanshao Zhu, Yanchuan Chang, Kang Luo, Haomin Wen, Lei Li, Yanwei Yu, Qingsong Wen, Chao Chen, Kai Zheng, Yunjun Gao, Xiaofang Zhou, and Yu Zheng. 2024. Deep Learning for Trajectory Data Management and Mining: A Survey and Beyond. arXiv:2403.14151 [cs.LG] <https://arxiv.org/abs/2403.14151>
- [10] Yuqi Chen, Hanyuan Zhang, Weitwei Sun, and Baihua Zheng. 2022. RNTrajRec: Road Network Enhanced Trajectory Recovery with Spatial-Temporal Transformer.
- [11] Anusuya Datta. 2022. Seizing The Future: Geospatial Industry Technology Trends and Directions. *GWPrime* (Feb 2022).
- [12] Ziquan Fang, Yuntao Du, Xinjun Zhu, Danlei Hu, Lu Chen, Yunjun Gao, and Christian S. Jensen. 2022. Spatio-Temporal Trajectory Similarity Learning in Road Networks. In *Proc. of the 28th ACM SIGKDD Conf. on Knowledge Discovery & Data Mining (ACM SIGKDD '22)*. 347–56.

- [13] Ali Faraji, Jing Li, Gian Alix, Mahmoud Alsaeed, Nina Yanin, Amirhossein Nadiri, and Manos Papagelis. 2023. Point2Hex: Higher-order Mobility Flow Data and Resources. In *Proc. of the 31st Intl. Conf. on Adv. in Geographic Info. Sys. (SIGSPATIAL '23)*.
- [14] William Fedus, Prajit Ramachandran, Rishabh Agarwal, Yoshua Bengio, Hugo Larochelle, Mark Rowland, and Will Dabney. 2020. Revisiting Fundamentals of Experience Replay. In *Proc. of the 37th Intl. Conf. on Machine Learning (ICML '20)*. JMLR, Article 287.
- [15] Yuanzhe Geng, Erwu Liu, Rui Wang, and Yiming Liu. 2020. Deep Reinforcement Learning Based Dynamic Route Planning for Minimizing Travel Time. *CoRR* (2020).
- [16] Ali Hamdi, Khaled Shaban, Abdelkarim Erradi, Amr Mohamed, Shakila Khan Rumi, and Flora D. Salim. 2022. Spatiotemporal data mining: a survey on challenges and open problems. *Artificial Intelligence Review* 55, 2 (Feb 2022), 1441–1488.
- [17] Nan Han, Shaojie Qiao, Kun Yue, Jianbin Huang, Qiang He, Tingting Tang, Faliang Huang, Chunlin He, and Chang-An Yuan. 2022. Algorithms for Trajectory Points Clustering in Location-Based Social Networks. *ACM Trans. Intell. Syst. Technol.* 13, 3, Article 43 (mar 2022).
- [18] Qingwen Han, Yu Lei, Lingqiu Zeng, Guangyan He, Lei Ye, and Lingfeng Qi. 2021. Research on Travel Time Prediction of Multiple Bus Trips Based on MDARNN. In *2021 IEEE Intl. Intelligent Transportation Sys. Conf. (ITSC)*. 3718–3725.
- [19] Conor F. Hayes, Roxana Rădulescu, Eugenio Bargiacchi, Johan Källström, Matthew Macfarlane, Mathieu Reymond, Timothy Verstraeten, Luisa M. Zintgraf, Richard Dazeley, and Fredrik Heintz. 2022. A Practical Guide to Multi-Objective Reinforcement Learning and Planning. *Autonomous Agents and Multi-Agent Systems* 36, 1 (April 2022). <https://doi.org/10.1007/s10458-022-09552-y>
- [20] Zhanjun He, Liufeng Tao, Zhong Xie, and Chong Xu. 2020. Discovering spatial interaction patterns of near repeat crime by spatial association rules mining. *Sci. Reports* 10, 1 (Oct 2020).
- [21] Zhengxing Lan, Hongbo Li, Lingshan Liu, Bo Fan, Yisheng Lv, Yilong Ren, and Zhiyong Cui. 2024. Traj-LLM: A New Exploration for Empowering Trajectory Prediction with Pre-trained Large Language Models. arXiv:2405.04909 [cs.CV] <https://arxiv.org/abs/2405.04909>
- [22] Jae-Gil Lee, Jiawei Han, and Kyu-Young Whang. 2007. Trajectory Clustering: A Partition-and-Group Framework. In *Proc. of the 2007 ACM SIGMOD Intl. Conf. on Mgt. of Data (ACM SIGMOD '07)*. 593–604.
- [23] Li Li, Rui Jiang, Zhengbing He, Xiquan (Michael) Chen, and Xuesong Zhou. 2020. Trajectory data-based traffic flow studies: A revisit. *Transportation Research Part C: Emerging Technologies* 114 (2020), 225–240.
- [24] Mingqian Li, Panrong Tong, Mo Li, Zhongming Jin, Jianqiang Huang, and Xian-Sheng Hua. 2021. Traffic Flow Prediction with Vehicle Trajectories. *Proceedings of the AAAI Conference on Artificial Intelligence* 35, 1 (May 2021), 294–302.
- [25] Tang Li, Jing Gao, and Xi Peng. 2021. Deep Learning for Spatiotemporal Modeling of Urbanization. In *Proc. of the 35th Conf. on Neural Info. Proc. Sys. (NeurIPS 2021)*.
- [26] Yang Li, Dimitrios Gunopulos, Cewu Lu, and Leonidas J. Guibas. 2019. Personalized Travel Time Prediction Using a Small Number of Probe Vehicles. *ACM Trans. Spatial Algorithms Syst.* 5, 1, Article 4 (may 2019).
- [27] Yin Lou, Chengyang Zhang, Yu Zheng, Xing Xie, Wei Wang, and Yan Huang. 2009. Map-Matching for Low-Sampling-Rate GPS Trajectories. In *Proc. of the 17th ACM SIGSPATIAL Intl. Conf. on Adv. in Geographic Info. Sys. (Seattle, Washington) (GIS '09)*. Assoc. for Comp. Machinery, New York, NY, USA, 352–361.
- [28] Ken McCormick. '97. An Essay on the Origin of the Rational Utility Maximization Hypothesis and a Suggested Modification. *Eastern Eco. Journal* 23 ('97), 17–30.
- [29] Saim Mehmood and Manos Papagelis. 2020. Learning Semantic Relationships of Geographical Areas based on Trajectories. In *2020 21st IEEE Intl. Conf. on Mobile Data Mgt. (MDM)*. 109–118.
- [30] Jonathan Muckell, Jeong-Hyon Hwang, Catherine T. Lawson, and S. S. Ravi. 2010. Algorithms for Compressing GPS Trajectory Data: An Empirical Evaluation. In *Proc. of the 18th SIGSPATIAL Intl. Conf. on Adv. in Geographic Info. Sys. (ACM GIS '10)*. 402–405.
- [31] Ali Nematichari, Tilemachos Pechlivanoglou, and Manos Papagelis. 2022. Evaluating and Forecasting the Operational Performance of Road Intersections. In *Proc. of the 30th Intl. Conf. on Adv. in Geographic Info. Sys. (ACM SIGSPATIAL '22)*. Article 31.
- [32] Mark E. J. Newman. 2018. *Networks* (second edition ed.). Oxford University Press, Oxford, United Kingdom; New York, NY, United States of America.
- [33] Paul Newson and John Krumm. 2009. Hidden Markov Map Matching through Noise and Sparseness. In *Proc. of the 17th ACM SIGSPATIAL Intl. Conf. on Adv. in Geographic Info. Sys. (GIS '09)*. 336–343.
- [34] Marguerite Nyhan, Sebastian Grauwinn, Rex Britter, Bruce Misstear, Aonghus McNabola, Francine Laden, Steven R. H. Barrett, and Carlo Ratti. 2016. “Exposure Track”—The Impact of Mobile-Device-Based Mobility Patterns on Quantifying Population Exposure to Air Pollution. *Environmental Science & Technology* 50, 17 (2016), 9671–9681.

- [35] Peter J. Olver and Chehrzad Shakiban. 2018. *Applied Linear Algebra* (2nd ed. 2018 ed.). Springer International Publishing: Imprint: Springer, Cham.
- [36] Costas Panagiotakis, Nikos Pelekis, Ioannis Kopanakis, Emmanuel Ramasso, and Yannis Theodoridis. 2012. Segmentation and Sampling of Moving Object Trajectories Based on Representativeness. *IEEE Trans. on Knowledge and Data Eng.* 24, 7 (2012), 1328–1343.
- [37] Manish Kumar Pandey, Prashant Srivastava, and George Petropoulos. 2021. Chapter 21 - Future pathway for research and emerging applications in GPS/GNSS. In *GPS and GNSS Technology in Geosciences*. Elsevier, 429–438.
- [38] Tilemachos Pechlivanoglou, Gian Alix, Nina Yanin, Jing Li, Farzaneh Heidari, and Manos Papagelis. 2022. Microscopic Modeling of Spatiotemporal Epidemic Dynamics. In *Proc. of the 3rd ACM SIGSPATIAL Intl. Workshop on Spatial Comp. for Epidemiology (SpatialEpi '22)*. 11–21.
- [39] Tilemachos Pechlivanoglou and Manos Papagelis. 2018. Fast and Accurate Mining of Node Importance in Trajectory Networks. In *2018 IEEE Intl. Conf. on Big Data (Big Data)*. 781–790.
- [40] Tom Ruth. 2022. Why Location Services and IoT are Leading the 5G Trends of 2022. *Quuppa* (Sep 2022).
- [41] Swaminathan Sankararaman, Pankaj K. Agarwal, Thomas Mølhave, Jiangwei Pan, and Arnold P. Boedihardjo. 2013. Model-Driven Matching and Segmentation of Trajectories. In *Proc. of the 21st ACM SIGSPATIAL Intl. Conf. on Adv. in Geographic Info. Sys. (Orlando, Florida) (SIGSPATIAL '13)*. Assoc. for Comp. Machinery, New York, NY, USA, 234–43.
- [42] Abdullah Sawas, Abdullah Abuolaim, Mahmoud Afifi, and Manos Papagelis. 2018. Tensor Methods for Group Pattern Discovery of Pedestrian Trajectories. In *19th IEEE Intl. Conf. on Mobile Data Mgt. (MDM)*. 76–85.
- [43] Abdullah Sawas, Abdullah Abuolaim, Mahmoud Afifi, and Manos Papagelis. 2019. A versatile computational framework for group pattern mining of pedestrian trajectories. *Geoinformatica* 23, 4 (Oct 2019), 501–531.
- [44] Artur Strzelecki. 2022. The Apple Mobility Trends Data in Human Mobility Patterns during Restrictions and Prediction of COVID-19: A Systematic Review and Meta-Analysis. *Healthcare* 10, 12 (2022).
- [45] Shao-Hua Sun, Te-Lin Wu, and Joseph J. Lim. 2020. Program Guided Agent. In *Intl. Conf. on Learning Representations*.
- [46] Marc van Kreveld and Lionov Wiratma. 2011. Median Trajectories Using Well-Visited Regions and Shortest Paths. In *Proc. of the 19th ACM SIGSPATIAL Intl. Conf. on Adv. in Geographic Info. Sys. (GIS '11)*. 241–250.
- [47] Kristof Van Moffaert, Madalina M. Drugan, and Ann Nowé. 2013. Scalarized Multi-Objective Reinforcement Learning: Novel Design Techniques. In *2013 IEEE Symposium on Adaptive Dynamic Programming and Reinforcement Learning (ADPRL)*. IEEE, Singapore. <https://doi.org/10.1109/ADPRL.2013.6615007>
- [48] Jingyuan Wang, Ning Wu, and Wayne Zhao. 2022. Personalized Route Recommendation With Neural Network Enhanced Search Algorithm. *IEEE Transactions on Knowledge & Data Engineering* 34, 12 (Dec 2022), 5910–5924.
- [49] Sheng Wang, Zhifeng Bao, J. Shane Culpepper, Timos Sellis, and Xiaolin Qin. 2019. Fast Large-Scale Trajectory Clustering. *Proc. VLDB Endow.* 13, 1 (Sep 2019), 29–42.
- [50] Senzhang Wang, Jiannong Cao, and Philip Yu. 2022. Deep Learning for Spatio-Temporal Data Mining: A Survey. *IEEE Trans. on Knowledge & Data Eng.* 34, 08 (Aug 2022), 3681–700.
- [51] Tingting Wang, Shixun Huang, Zhifeng Bao, J. Shane Culpepper, and Reza Arablouei. 2022. Representative Routes Discovery from Massive Trajectories. In *Proc. of the 28th ACM SIGKDD Conf. on Knowledge Discovery and Data Mining (Washington DC, USA) (KDD '22)*. Assoc. for Comp. Machinery, New York, NY, USA, 4059–69.
- [52] Zheng Wang, Cheng Long, and Gao Cong. 2021. Trajectory Simplification with Reinforcement Learning. In *2021 IEEE 37th Intl. Conf. on Data Eng. (ICDE)*. 684–695.
- [53] Zhaobo Wang, Yanmin Zhu, Qiaomei Zhang, Haobing Liu, Chunyang Wang, and Tong Liu. 2022. Graph-Enhanced Spatial-Temporal Network for Next POI Recommendation. *ACM Trans. Knowl. Discov. Data* 16, 6, Article 104 (Jul 2022).
- [54] Jiajie Xu, Jing Zhao, Rui Zhou, Chengfei Liu, Pengpeng Zhao, and Lei Zhao. 2021. Predicting Destinations by a Deep Learning based Approach. *IEEE Trans. on Knowledge and Data Eng.* 33, 2 (2021), 651–666.
- [55] Hao Xue, Bhanu Prakash Voutharoja, and Flora D. Salim. 2022. Leveraging Language Foundation Models for Human Mobility Forecasting. In *Proc. of the 30th Intl. Conf. on Adv. in Geographic Info. Sys. (ACM SIGSPATIAL '22)*. Article 90.
- [56] R. K. Yadav, Giriraj Kishor, Himanshu, and Kishan Kashyap. 2020. Comparative Analysis of Route Planning Algorithms on Road Networks. In *2020 5th Intl. Conf. on Comm. and Electronics Sys. (ICCES)*. 401–406.
- [57] Mohamad Yassin and Elias Rachid. 2015. A survey of positioning techniques and location based services in wireless networks. In *2015 IEEE Intl. Conf. on Signal Processing, Informatics, Communication and Energy Systems (SPICES)*. 1–5.
- [58] Jing Yuan, Yu Zheng, Chengyang Zhang, Xing Xie, and Guang-Zhong Sun. 2010. An Interactive-Voting Based Map Matching Algorithm. In *2010 11th Intl. Conf. on Mobile Data Mgt.* 43–52.
- [59] Jing Zhao, Jiajie Xu, Rui Zhou, Pengpeng Zhao, Chengfei Liu, and Feng Zhu. 2018. On Prediction of User Destination by Sub-Trajectory Understanding: A Deep Learning Based Approach. In *Proc. of the 27th ACM Intl. Conf. on Info. and Knowledge Mgt. (ACM CIKM 2018)*. 1413–1422.
- [60] Yan Zhao, Shuo Shang, Yu Wang, Bolong Zheng, Quoc Viet Hung Nguyen, and Kai Zheng. 2018. REST: A Reference-Based Framework for Spatio-Temporal Trajectory Compression. In *Proc. of the 24th ACM SIGKDD Intl. Conf. on Knowledge Discovery & Data Mining (ACM SIGKDD '18)*. 2797–2806.

- [61] Yaya Zhao, Kaiqi Zhao, Zhiqian Chen, Yuanyuan Zhang, Yalei Du, and Xiaoling Lu. 2024. A Graph-based Representation Framework for Trajectory Recovery via Spatiotemporal Interval-Informed Seq2Seq. In *Proceedings of the Thirty-Third International Joint Conference on Artificial Intelligence, IJCAI-24*, Kate Larson (Ed.). International Joint Conferences on Artificial Intelligence Organization, 2588–2597. <https://doi.org/10.24963/ijcai.2024/286> Main Track.
- [62] Yu Zheng. 2015. Trajectory Data Mining: An Overview. *ACM Trans. Intell. Syst. Technol.* 6, 3, Article 29 (May 2015).
- [63] Yue Zhou and Thomas S. Huang. 2008. ‘Bag of segments’ for motion trajectory analysis. In *2008 15th IEEE Intl. Conf. on Image Processing*. 757–760.
- [64] Yuanshao Zhu, Yongchao Ye, Shiyao Zhang, Xiangyu Zhao, and James J. Q. Yu. 2023. DiffTraj: Generating GPS Trajectory with Diffusion Probabilistic Model. arXiv:2304.11582 [cs.LG] <https://arxiv.org/abs/2304.11582>

APPENDIX

A PATHLET DICTIONARY'S APPLICATIONS

Trajectory Compression. Compression is the process of reducing the size of a trajectory while preserving its important spatiotemporal features [30]; it is more commonly useful when there is a need of transmitting or storing large trajectory datasets in much smaller, more limited resources (e.g., mobile devices, wireless networks, etc.). A common technique for trajectory compression involves sampling points in trajectories that carry the most significant amount of spatiotemporal information. With a pathlet dictionary, we are able to capture the pathlets in a trajectory's pathlet-based representation set that are most useful and could represent a large number of trajectories in the dataset.

Route Planning. While navigation services and route planning apps such as Google Maps⁹ and Apple Maps¹⁰ exist, they are not necessarily accessible to users when online (internet) connection is not available (e.g., network outages, poor wifi signals in remote areas, etc.). As such, there is a need for accessing maps and loading mobility data offline while at the same time efficiently answering majority of user queries (for example, path recommendation from Point A to B). Pathlet dictionaries can be useful in this case.

Trajectory Prediction. Prediction and forecasting of trajectories is important in several domains including transportation [23], urban planning [25], and healthcare [38, 44]. Pathlets could be useful by expressing trajectories as sequences of pathlets, predicting the next pathlet(s) in the sequence and then concatenating these predicted pathlets to form the predicted trajectories.

Anomaly Detection. Spotting outliers has been an active research direction. One could use pathlets to detect trajectories that move or behave anomalously by expressing each trajectory as their pathlet-based representation set and then identifying which of those trajectories has a pathlet-based representation set that deviates from other trajectories.

Trajectory Similarity Search. The trajectory similarity search task is an important problem of interest due to its numerous practical applications in domains such as traffic analysis [24], public safety [20], and environmental conservation [34]. With pathlets, the similarity of two trajectories can be calculated based on the cosine similarity (or some other similarity metric) of their pathlet-based representations.

B PROOF OF THEOREM 3.1

Before proceeding with the proof, we first introduce two facts that will prove useful in our main proof for the theorem.

Fact 1. The pathlet length of some pathlet $\rho_A \in \mathcal{P}$, plus the pathlet length of a neighboring pathlet $\rho_B \in \mathcal{P}$ is equal to the pathlet length of ρ_{AB} , where ρ_{AB} is the pathlet formed when pathlets ρ_A and ρ_B are merged. In other words:

$$\ell(\rho_A) + \ell(\rho_B) = \ell(\rho_{AB}) \quad (6)$$

This fact is fairly intuitive and does not require further explanation. Note that either one of ρ_A or ρ_B (or both) has length 1¹¹.

⁹<http://maps.google.com/>

¹⁰<https://www.apple.com/maps/>

¹¹This is because we would never find two higher-ordered (i.e., a pathlet with length greater than 1) pathlets merging together. The current pathlet in process can only merge with a neighboring pathlet that have never been processed in the algorithm (they all have length 1) and any neighboring high-ordered pathlets have already been preprocessed and added to the dictionary.

Fact 2. The sequence of trajectory representabilities $\{\mu_i\}$ for some trajectory $\tau \in \mathcal{T}$ is monotonically non-increasing. In other words, the trajectory representability of τ at some iteration j of the algorithm, for some $i < j$ is less than or equal to its representability at iteration i :

$$\mu_i(\tau) \geq \mu_j(\tau) \quad (7)$$

This claim is straightforward and intuitive as it simply stems from the nature of Algorithm ???. As a remark, if $j = i + 1$, then $\mu_i(\tau) \geq \mu_{i+1}(\tau)$. This then implies that:

$$\mu_i(\tau) = \mu_{i+1}(\tau) + \epsilon \quad (8)$$

for some non-negative $\epsilon \geq 0$.

Proof of Theorem 3.1.

We are then ready to provide proof to this theorem by means of induction. First, we claim that the theorem holds at the initial base case, i.e., when $i = 0$:

$$\mu_0(\tau) = \frac{\sum_{\rho' \in \Phi_0(\tau)} \ell(\rho')}{\sum_{\rho \in \Phi_0(\tau)} \ell(\rho)} = 1 = 100\%$$

which checks out since the trajectory representabilities of all trajectories $\tau \in \mathcal{T}$ have this representability value at the beginning of the algorithm. Now, assume that the theorem holds at some iteration $i = n \geq 0$:

$$\mu_n(\tau) = \frac{\sum_{\rho' \in \Phi_n(\tau)} \ell(\rho')}{\sum_{\rho \in \Phi_0(\tau)} \ell(\rho)}$$

All it remains to complete the proof is to show that the theorem holds for when $i = n + 1$, i.e.,

$$\mu_{n+1}(\tau) = \frac{\sum_{\rho' \in \Phi_{n+1}(\tau)} \ell(\rho')}{\sum_{\rho \in \Phi_0(\tau)} \ell(\rho)}$$

Now let current pathlet ρ_A be the pathlet that merges with its neighbor pathlet ρ_B to form ρ_{AB} at the iteration $(n + 1)$. At this point, there are three cases to consider.

Case 1. $\rho_A \notin \Phi_n(\tau)$ and $\rho_B \notin \Phi_n(\tau)$

This is the case when both these two pathlets that are candidate for merging are not in the pathlet-based representation set $\Phi_n(\tau)$. This means that there is no change to the pathlet-based representation of τ from iteration n to $(n+1)$; i.e., $\Phi_{n+1}(\tau) = \Phi_n(\tau)$, as well as their representabilities at iteration $(n + 1)$, i.e., $\mu_{n+1}(\tau) = \mu_n(\tau)$.

$$\mu_{n+1}(\tau) = \mu_n(\tau) = \frac{\sum_{\rho' \in \Phi_n(\tau)} \ell(\rho')}{\sum_{\rho \in \Phi_0(\tau)} \ell(\rho)} = \frac{\sum_{\rho' \in \Phi_{n+1}(\tau)} \ell(\rho')}{\sum_{\rho \in \Phi_0(\tau)} \ell(\rho)}$$

Case 2. $\rho_A \in \Phi_n(\tau)$ and $\rho_B \in \Phi_n(\tau)$

In this case, both ρ_A and ρ_B are in $\Phi_n(\tau)$ and therefore their merged pathlet ρ_{AB} will be in the pathlet-based representation of τ at the next iteration $(n + 1)$, i.e., $\rho_{AB} \in \Phi_{n+1}(\tau)$. Note that that both ρ_A and ρ_B will no longer be in $\Phi_{n+1}(\tau)$. Moreover in this case, it is clear as well that their

representabilities of τ also do not change between iterations n and $(n + 1)$. Thus we have:

$$\begin{aligned}
\mu_{n+1}(\tau) &= \mu_n(\tau) \\
&= \frac{\sum_{\rho' \in \Phi_n(\tau)} \ell(\rho')}{\sum_{\rho \in \Phi_0(\tau)} \ell(\rho)} && \text{(by the Inductive Hypothesis)} \\
&= \frac{\sum_{\rho' \in \Phi_n(\tau) \setminus \{\rho_A, \rho_B\}} \ell(\rho') + \ell(\rho_A) + \ell(\rho_B)}{\sum_{\rho \in \Phi_0(\tau)} \ell(\rho)} && \text{(separate } \rho_A \text{ and } \rho_B) \\
&= \frac{\sum_{\rho' \in \Phi_n(\tau) \setminus \{\rho_A, \rho_B\}} \ell(\rho') + \ell(\rho_{AB})}{\sum_{\rho \in \Phi_0(\tau)} \ell(\rho)} && \text{(by Fact 1)} \\
&= \frac{\sum_{\rho' \in \Phi_n(\tau) \setminus \{\rho_A, \rho_B\} \cup \{\rho_{AB}\}} \ell(\rho')}{\sum_{\rho \in \Phi_0(\tau)} \ell(\rho)} && \text{(inclusion of the new merged pathlet } \rho_{AB}) \\
&= \frac{\sum_{\rho' \in \Phi_{n+1}(\tau)} \ell(\rho')}{\sum_{\rho \in \Phi_0(\tau)} \ell(\rho)} && \text{(as } \Phi_{n+1}(\tau) = \Phi_n(\tau) \setminus \{\rho_A, \rho_B\} \cup \{\rho_{AB}\})
\end{aligned}$$

Note that in the last step, to get $\Phi_{n+1}(\tau)$, this is simply the same as the previous $\Phi_n(\tau)$ except we take out the two pathlets that are candidate for merging $\{\rho_A, \rho_B\}$ and then add back the newly formed merged pathlet $\{\rho_{AB}\}$.

Case 3. $\rho_A \in \Phi_n(\tau)$ and $\rho_B \notin \Phi_n(\tau)$

Without loss of generality, this case should suffice for when only one of $\{\rho_A, \rho_B\}$ is in $\Phi_n(\tau)$. Unlike Cases 1 and 2 where the representability of τ did not change, here in Case 3 τ 's representability will decrease. Following from Fact 2, there exists some positive $\epsilon > 0$ that satisfies the equality in Equation (8). This equation can be rewritten as:

$$\mu_{n+1}(\tau) = \mu_n(\tau) - \epsilon \quad (*)$$

(where i 's are expressed as n 's). From here, it is not difficult to see that the ϵ we are after is basically the percentage of the trajectory that can no longer be represented by the pathlets in the dictionary at the next iteration $(n + 1)$. Since we know that ρ_A , which was part of $\Phi_n(\tau)$ will no longer be part of $\Phi_{n+1}(\tau)$ due to its merge with ρ_B to form ρ_{AB} (and moreover, ρ_{AB} is not part of $\Phi_{n+1}(\tau)$ as $\rho_B \notin \Phi_n(\tau)$), then it must be that the portion covered by ρ_A in τ is the loss and is the ϵ that we want:

$$\epsilon = \frac{\ell(\rho_A)}{\sum_{\rho \in \Phi_0(\tau)} \ell(\rho)} > 0 \quad (**)$$

Note that this value is positive as both $\ell(\rho_A) > 0$ and $\sum_{\rho \in \Phi_0(\tau)} \ell(\rho) > 0$. So now we have:

$$\begin{aligned}
\mu_{n+1}(\tau) &= \mu_n(\tau) - \epsilon && \text{(by (*))} \\
&= \frac{\sum_{\rho' \in \Phi_n(\tau)} \ell(\rho')}{\sum_{\rho \in \Phi_0(\tau)} \ell(\rho)} - \epsilon && \text{(by the Inductive Hypothesis)} \\
&= \frac{\sum_{\rho' \in \Phi_n(\tau)} \ell(\rho')}{\sum_{\rho \in \Phi_0(\tau)} \ell(\rho)} - \frac{\ell(\rho_A)}{\sum_{\rho \in \Phi_0(\tau)} \ell(\rho)} && \text{(by (**))} \\
&= \frac{\sum_{\rho' \in \Phi_n(\tau)} \ell(\rho') - \ell(\rho_A)}{\sum_{\rho \in \Phi_0(\tau)} \ell(\rho)} \\
&= \frac{\sum_{\rho' \in \Phi_n(\tau) \setminus \{\rho_A\}} \ell(\rho') + \ell(\rho_A) - \ell(\rho_A)}{\sum_{\rho \in \Phi_0(\tau)} \ell(\rho)} && \text{(separate } \rho_A) \\
&= \frac{\sum_{\rho' \in \Phi_n(\tau) \setminus \{\rho_A\}} \ell(\rho')}{\sum_{\rho \in \Phi_0(\tau)} \ell(\rho)} \\
&= \frac{\sum_{\rho' \in \Phi_{n+1}(\tau)} \ell(\rho')}{\sum_{\rho \in \Phi_0(\tau)} \ell(\rho)} && \text{(as } \Phi_{n+1}(\tau) = \Phi_n(\tau) \setminus \{\rho_A\})
\end{aligned}$$

Thus, on the basis of the inductive hypothesis, we just have shown that:

$$\mu_{n+1}(\tau) = \frac{\sum_{\rho' \in \Phi_{n+1}(\tau)} \ell(\rho')}{\sum_{\rho \in \Phi_0(\tau)} \ell(\rho)}$$

Clearly, the theorem holds true for all $i \geq 0$, which completes the proof. \square

C SPACE COMPLEXITY ANALYSIS

To analyze the space complexity expressed in terms of the n number of road segments on the road network, we can simply provide a lower bound on this number. First, we consider the analysis for top-down approaches. The following two facts would be useful in this proof (we will bypass the proofs of these facts as they are trivial; refer to linear algebra books for their complete proofs [35]).

Fact 1. Let a_{ij} be the entry situated at the i th row and j th column of an $m \times m$ square matrix A . Moreover, let \mathbf{x} be a column vector of ones that has dimension $m \times 1$. Then the sum of all entries of A is:

$$\sum_{i=1}^m \sum_{j=1}^m a_{ij} = \mathbf{x}^T A \mathbf{x} \quad (9)$$

Fact 2. For an $m \times m$ square symmetric matrix A (i.e., $A = A^T$) with λ_{min} as its smallest eigenvalue, then the quadratic form $\mathbf{x}^T A \mathbf{x}$ is lower bounded by the squared L_2 -norm of \mathbf{x} , for all $\forall \mathbf{x} \in \mathbb{R}^{m \times 1}$:

$$\mathbf{x}^T A \mathbf{x} \geq \lambda_{min} \|\mathbf{x}\|_2^2 \quad (10)$$

In other words, $\mathbf{x}^T A \mathbf{x} \in \Omega(\|\mathbf{x}\|_2^2)$

Space Complexity Analysis. So now we focus firstly on the nodes (road intersections) of the road network. If one was to construct an adjacency matrix A where entry $a_{ij} \in A$ equals 1 if there is an edge (or road segment) from i to j (or j to i as our road network is undirected by assumption) and 0 otherwise, then $a_{ij} \in A^\ell$ determines the number of paths of length ℓ to traverse node i to j (or vice-versa) on the road network represented by adjacency matrix A [32]. Assuming the absence of self-loops, then the total number of paths of length ℓ for any pair of nodes in the road network is the sum of all entries in the upper diagonal (excluding the main diagonal) of A^ℓ . We express it as follows. Let $Q_\ell = A^\ell - \mathcal{D}(A^\ell)$, where $\mathcal{D}(A)$ is the matrix that contains the diagonal entries of A

along its main diagonal and zeros elsewhere. And then the sum of the upper diagonal entries of Q_ℓ is simply $\frac{1}{2}\mathbf{x}^\top Q_\ell \mathbf{x}$, with \mathbf{x} as $\dim(A) \times 1$ column of ones (the sum of entries is in line with Fact 1 above in Equation (9)). And then the half here is to avoid double counting (i.e., the undirected graph from i to j is the same as j to i as a result of symmetry). So clearly, if we want all the pathlets of at least length-1, then we can write it as follows:

$$\sum_{\substack{\ell \in \mathbb{Z}^+ \\ \mathbf{x}^\top Q_\ell \mathbf{x} \neq 0}} \frac{1}{2} \mathbf{x}^\top Q_\ell \mathbf{x} \quad (11)$$

To yield a lower bound on this summation with respect to the number of road segments in the road network (instead of the nodes/road intersections), consider the smallest possible number of nodes for n edges in the road network first. Each edge connects together two nodes; as a result, there can be at least $|\mathcal{V}| = n$ nodes (i.e., $\dim(A) = n$). Thus, in Equation (11), (assuming we have this least possible number of nodes) then it turns out that the $\dim(Q_\ell) = n$ and $\dim(\mathbf{x}) = n \times 1$ as a result of $\dim(A) = n$.

Now, each of the terms in the summation of Equation (11) is lower-bounded by $\Omega(\|\mathbf{x}\|_2^2) = \Omega(n)$ as a consequence of the Fact 2 in Equation (10). To see why $\Omega(\|\mathbf{x}\|_2^2)$ reduces to $\Omega(n)$, first note that \mathbf{x} is a column vector of ones with dimension $n \times 1$. Therefore, its squared L_2 -norm is: $(\sqrt{1^2 + 1^2 + \dots + 1^2})^2 = (\sqrt{n})^2 = n$. Note however that the eigenvalue λ_{min} should not be relevant towards the space complexity expressed in terms of the number of road segments. However, such space analysis is only for one of the n terms in the summation of Equation (11)¹²; thus the lower bound for the number of pathlets of the top-down scheme is $n \times \Omega(n) = \Omega(n^2)$.

On the other hand, the proposed bottom-up method PATHLET-RL, which consumes less memory space to initially store the pathlets, is more efficient with $\Theta(n)$ memory space complexity. It is quite easier to analyze. Since we only consider length-1 edge-disjoint pathlets, it is easy to see how ours simply relies exactly on the number of segments in the road network – which happens to be n , and is therefore more space efficient compared to the top-down approaches the requires at least $\Omega(n^2)$ amount of memory space. \square

D MAP-MATCHING

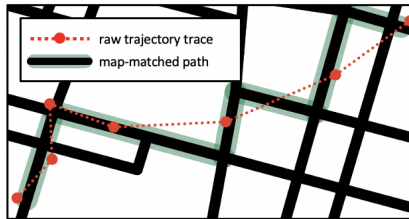


Fig. 14. An example of the map-matching procedure.

Map-matching is a common task that identifies the path on the road an object has taken given a sequence of GPS locations [33] (Fig. 14 provides an illustrative example). Ideally, we prefer highly accurate map-matched data from GPS trajectory traces; however, this task is itself involved and is outside the paper's scope. Thus, we rely on existing methods [27, 58] to handle map-matching.

¹²It can be noted that at the worst case, the longest pathlet length in the road network is n ; so that is why the summation can have up to n terms

E OTHER DEEP REINFORCEMENT LEARNING POLICIES

The choice of DQN method over others such as Actor-Critic (A2C) and Policy-gradient is due to a number of reasons. For one, DQNs are more sample efficient than Policy-gradient methods because learning happens using an experience replay buffer rather than learning from data collected with the current policy. Moreover, with small action spaces, DQN’s are more stable and more efficient than A2C methods; a separate neural network computes (approximates) the target Q -values, which can reduce the variance in these estimates. In addition, implementing DQNs is more straightforward compared to Actor-critic and Policy-gradient methods that tend to be more complex in terms of architectures and hyperparameter tuning. This makes them easier to employ in real-world settings.

F DATASET STATISTICS

	Feature	TORONTO	ROME
roadmap	# nodes	1.9K	7.5K
	# edges / initial pathlets	2.5K	15.4K
trajectories	Trajectory type	realistic synthetic	real world
	Object	cars	taxis
	# Total geolocation data points	169K	3.8M
	# Total trajectories	2.9K	75K

Table 7. Dataset attributes

G PRIVACY AND ETHICS

Our proposed methodology makes use of real-world trajectory datasets in the experiments that could potentially raise concerns about the individual (vehicle taxi cab) privacy and the potential for re-identification of such individuals. Therefore, to ensure protection of privacy and ethical considerations, all datasets used in our evaluation have been anonymized. Such datasets are derived from publicly-available sources, are publicly available, and are free of use for the intention of research purposes as outlined by their curators. In addition, all terms and conditions of use have been followed, with proper attribution and citation of works.

H IMPLEMENTATION DETAILS

Machine Specifications. We conducted experiments on a server equipped with an NVIDIA RTX A6000 graphics card and 320GB of memory.

The RL Implementation. We implemented our deep reinforcement learning architecture using the `stable-baselines3`¹³ package, a PyTorch-based library designed specifically for implementing RL methods.

I THE CHOICE OF BASELINES

While there have been a number of considerable baseline methods [36, 51, 63] that can be used to compare PATHLETRL with, there are some reasons we decided to not do so. Firstly, Wang et al. [51] focuses on route representativeness discovery which is a completely different task than ours. Theirs, including Panagiotakis et al. [36] use a representativeness criterion that is not applicable to our case. Zhou et al. [63] moreover focuses on motion analysis which is a substantially different setting

¹³<https://stable-baselines3.readthedocs.io>

and task. This is in contrast to Chen et al. [8] and Agarwal et al. [1], where we have opted for their baselines methods due to a number of reasons. The former is the original and most representative work on pathlet dictionary construction, while the latter is the most representative/newest method on subtrajectory clustering that frames the pathlet dictionary construction as a subtrajectory clustering task. Both of these baselines also do not rely on learning-based methods, compared to our proposed model where we show the importance of deep learning.

As an aside, it is important to note that the technical problem of trajectory pathlet dictionary construction is novel and state-of-the-art methods are originating from the original work of Chen et al. [8]. We revisit the problem with a RL-based approach and consider additional constraints (such as edge-disjointness in pathlets and the k -order constraint).